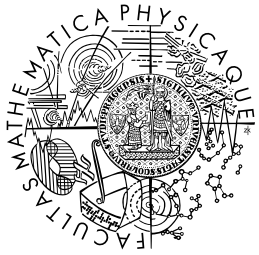

FACULTY
OF MATHEMATICS
AND PHYSICS
Charles University

DOCTORAL THESIS

Ondřej Kincl

Extension of smoothed particle hydrodynamics based on Poisson brackets

Mathematical Institute of Charles University

Supervisor of the doctoral thesis: doc. RNDr. Michal Pavelka, Ph.D.

Study programme: Mathematical and computer modeling

Study branch: P4F11

Prague 2023

I declare that I carried out this doctoral thesis independently, and only with the cited sources, literature and other professional sources. It has not been used to obtain another or the same degree.

I understand that my work relates to the rights and obligations under the Act No. 121/2000 Sb., the Copyright Act, as amended, in particular the fact that the Charles University has the right to conclude a license agreement on the use of this work as a school work pursuant to Section 60 subsection 1 of the Copyright Act.

In ..... date ....

Author's signature

Title: Extension of smoothed particle hydrodynamics based on Poisson brackets

Author: Ondřej Kincl

Institute: Mathematical Institute of Charles University

Supervisor: doc. RNDr. Michal Pavelka, Ph.D., Mathematical Institute of Charles University

Abstract: The thesis aims to find a generalization of smoothed particle hydrodynamics to fluid models which are compatible with Hamiltonian formulation of physics. We develop an approach based on a particle discretization of Poisson brackets. The main advantage of this approach is easy verification of conservation laws, which are related to the degree of consistency of discrete derivatives. Firstly, we demonstrate our technique on a particle approximation of symmetric hyperbolic thermodynamically compatible equations, which allow for unified description of fluids, viscoelastic materials and solids. Secondly, we develop a novel particle approximation for superfluid helium-4.

Keywords: Smoothed Particle Hydrodynamics SHTC equations Superfluid helium

Contents

Introduction

Smoothed particle hydrodynamics is a numerical method used to solve partial differential equations. It originated in the field of astrophysics [1]. Being Lagrangian and mesh-free, the method is particularly useful for simulations of free surface flows. Moreover, SPH s relatively simple to implement and conserves energy, linear and angular momentum. Among the caveats of SPH are slower convergence rate and numerical artifacts like particle clumps or tensile instability [2].

SPH is primarily a method for hydrodynamical problems described by Navier-Stokes system and was also successfully extended to elastic solids [3]. The novelty and purpose of the thesis is to use the SPH machinery to derive conservative schemes for various equations which arise from the Hamiltonian formulation of physics.

We remind that in Hamiltonian formulation, evolution of any functional A in phase variables and time is determined by

$$\frac{\mathrm{d}A}{\mathrm{d}t} = \frac{\partial A}{\partial t} + \{A, \mathcal{H}\}\,, \tag{1}$$

where $\mathcal{H}$ is the Hamiltonian (often identical with the total energy) and $\{\cdot,\cdot\}$ is a Poisson bracket. In general, Poisson bracket is a bilinear form, which satisfies the following constraints:

- Anti-symmetry: $\{A, B\} = -\{B, A\}$
- Jacobi identity: $\{A, \{B, C\}\} + \{B, \{C, A\}\} + \{C, \{A, B\}\} = 0$
- Leibniz rule: $\{A, BC\} = B\{A, C\} + C\{A, B\}$

for any fields A, B, C. In finite-dimensional canonical coordinates (generalized coordinates q_i and momenta p_i), the Poisson bracket takes the form

$$\{A, B\} = \sum_i \left(\frac{\partial A}{\partial q_i}\frac{\partial B}{\partial p_i} - \frac{\partial B}{\partial q_i}\frac{\partial A}{\partial p_i} \right) \tag{2}$$

which is called *canonical bracket*. The combination of (1) and (2) leads to well known Hamilton's equations. The formulation with Poisson brackets is, however, coordinate-free and more general. In the Hamiltonian formulation, conservation laws are related to the differentiable symmetries of Hamiltonian by Noether's theorem [4]. The simplest example is the conservation of energy ($\frac{\mathrm{d}\mathcal{H}}{\mathrm{d}t} = 0$), which can be understood as a consequence of translational time-symmetry of Hamiltonian ($\frac{\mathrm{d}\mathcal{H}}{\mathrm{d}t} = 0$) and the anti-symmetry of the Poisson bracket.

Still, the equation (1) accounts only for reversible processes. In GENERIC (General Equation for Nonlinear Equilibrium Reversible-Irreversible Coupling), irreversible phenomena are included using gradient dynamics. This approach is automatically consistent with conservation laws and also guarantees entropic inequality for smooth solutions [5].

In this thesis, we use the GENERIC to obtain particle approximations by finding a discrete analogue of the corresponding Poisson bracket. Thus, we can

easily extend SPH to non-standard fluid equations. By virtue of the construction, the approximate solution will satisfy discrete conservation laws (up to time-discretization error and round-off).

The work is structured as follows: In the first chapter, we explain the fundamentals of SPH and provide some theoretical insights. This introductory chapter is a compilation of research from other authors. In the second chapter, we will be interested in the SHTC (Symmetric Hyperbolic Thermodynamically Compatible) model — a system of equations introduced by Peshkov and Romensky, which offers a unified description of fluid and solid dynamics. This chapter lays foundations of new (and presumable the first) particle approach to SHTC model. Finally, in the third chapter, we focus on superfluid dynamics of liquid ^{4}He. We demonstrate our novel particle approximation on simulation of second sound waves and superfluid fountain effect to excellent agreement with theoretical predictions.

The thesis is extensive summary of our results published in papers [6, 7, 8].

1. SPH method

1.1 Smoothing kernels

Let us first recall the standard construction of SPH: The continuum is approximated by N particles, where each particle $a \in \{1 \dots N\}$ has its position $\boldsymbol{x}_a$, mass m_a, velocity $\boldsymbol{v}_a$, density ρ_a, etc. These particles are advected by the fluid, which means that $\dot{\boldsymbol{x}}_a = \boldsymbol{v}_a$. The second ingredient of SPH is a *smoothing kernel* $W_h : \mathbb{R}^d \to [0, \infty)$, a function with the following properties:

- $\int W_h(\boldsymbol{x}) \, \mathrm{d}\boldsymbol{x} = 1$
- $W_h \in C^2(\mathbb{R}^d)$
- $W_h = W_h(|\boldsymbol{x}|)$
- h: $W_h(r) = \frac{1}{h^d} W_1\left(\frac{r}{h}\right)$
- $\frac{\mathrm{d}W_h}{\mathrm{d}r} \leq 0$

Parameter $h > 0$ is called *smoothing length*. Function W_h converges to Dirac delta when $h \to 0^+$ (in distributional sense). Typically, the kernel has a bell-shaped structure as illustrated in Figure 1.1.

Partial derivatives are discretized using a two-step procedure. Firstly, we approximate $\partial_i f$ (where f represents any unknown variable appearing in the equations) using convolution henceforthly:

$$\partial_i f = \partial_i f * \delta \approx \partial_i f * W_h = f * \partial_i W_h. \tag{1.1}$$

Secondly, we approximate this convolution using a quadrature rule with nodes $\boldsymbol{x}_a$ and weights $V_a = m_a/\rho_a$. This leads to the following expression:

$$[f * \partial_i W_h](\boldsymbol{x}_a) = \int f(\boldsymbol{y}) \, \partial_i W_h(\boldsymbol{x} - \boldsymbol{y}) \, \mathrm{d}\boldsymbol{y} \approx \sum_b V_b f_b \, \partial_i W_{h,ab} \tag{1.2}$$

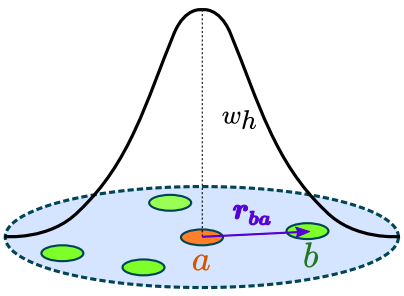

Figure 1.1: A scheme explaining SPH in a two dimensional setting. Derivatives are approximated using a kernel, which gives weights to interactions between particles.

where $f_b = f(\boldsymbol{x}_b)$ and

$$\nabla W_{h,ab} = \nabla W_h(\boldsymbol{x}_a - \boldsymbol{x}_b) = \frac{\mathrm{d}W_h}{\mathrm{d}r}(|\boldsymbol{x}_a - \boldsymbol{x}_b|)\frac{\boldsymbol{x}_a - \boldsymbol{x}_b}{|\boldsymbol{x}_a - \boldsymbol{x}_b|}. \tag{1.3}$$

Theoretical accuracy of this approximation will be discussed in Section 1.3. An important property of the kernel gradient, which we will use repeatedly, is the odd symmetry with respect to particle labels:

$$\nabla W_{h,ab} = -\nabla W_{h,ba} \tag{1.4}$$

One possible kernel choice is the Gaussian kernel

$$W_h(r) = \frac{1}{(2\pi h^2)^{\frac{d}{2}}} \exp\left(\frac{r^2}{h^2}\right), \quad \forall r \geq 0, \tag{1.5}$$

which is used, for example, in [9]. However, this kernel has the disadvantage of having infinite support, which means that the sum in (1.2) has to be made over all particles in the domain, which is computationally inefficient. Additionally, evaluating an exponential function is relatively expensive. For this reason, piece-wise polynomial kernels with compact support are often used. A canonical example of compactly supported kernel is the Wendland's quintic kernel [10]:

$$W_h(r) = \begin{cases} \frac{\alpha_d}{h^d}\left(1 - \frac{r}{2h}\right)^4\left(1 + \frac{4r}{h}\right) & 0 \leq r \leq 2h \\ 0 & 2h < r \end{cases}, \tag{1.6}$$

where normalization constant α_d is

$$\alpha_d = \begin{cases} \frac{3}{4} & d = 1 \\ \frac{7}{4\pi} & d = 2 \\ \frac{21}{16\pi} & d = 3 \end{cases}. \tag{1.7}$$

Another possibility is the quartic spline [11]

$$W_h(r) = \frac{\alpha_d}{h^d} \times \begin{cases} \left(\frac{5}{2} - \frac{r}{h}\right)^4 - 5\left(\frac{3}{2} - \frac{r}{h}\right)^4 + 10\left(\frac{1}{2} - \frac{r}{h}\right)^4 & 0 < r \leq \frac{h}{2} \\ \left(\frac{5}{2} - \frac{r}{h}\right)^4 - 5\left(\frac{3}{2} - \frac{r}{h}\right)^4 & \frac{h}{2} < r \leq \frac{3h}{2} \\ \left(\frac{5}{2} - \frac{r}{h}\right)^4 & \frac{3h}{2} < r \leq \frac{5h}{2} \\ 0 & \frac{5h}{2} < r \end{cases}, \tag{1.8}$$

where

$$\alpha_d = \begin{cases} \frac{1}{24} & d = 1 \\ \frac{96}{1199\pi} & d = 2 \\ \frac{1}{20\pi} & d = 3 \end{cases}. \tag{1.9}$$

For more kernel examples, we refer to [12].

In the Fourier image, we have:

$$\mathcal{F}\left(\partial_i f * W_h\right) = \hat{W}_h \mathcal{F}(\partial_i f), \tag{1.10}$$

where $\hat{W}_h$ satisfies

- $\hat{W}_h(0) = 1$,
- $\hat{W}_h(+\infty) = 0$,
- $\hat{W}_h(\xi) = \hat{W}_1(h\xi)$.

The kernel gives weights to $\mathcal{F}(\partial_i f)$ such that the amplitude of low frequency waves ($\xi \ll \frac{1}{h}$) is unchanged while high frequency waves ($\xi \gg \frac{1}{h}$) are damped. As $h \to 0^+$, the kernel W_h becomes increasingly concentrated around the origin, converging to Dirac delta in distributional topology. On the other hand, $\hat{W}_h$ becomes increasingly spread out, converging to a constant function 1. Therefore, mollifying by smoothing kernels can be understood as an attenuation of high frequency signals (which cannot be resolved faithfully for finite number of particles).

1.2 Inviscid particle approximation

An isentropic compressible fluid is described by the following system of equations:

$$\begin{aligned} \dot{\rho} &= -\rho \operatorname{div} \boldsymbol{v}, \\ \dot{\boldsymbol{v}} &= -\frac{\nabla p}{\rho}, \end{aligned} \tag{1.11}$$

where $\rho, \boldsymbol{v}$ are density and Eulerian velocity field and $\cdot$ denotes the convective derivative. We omit external forces like gravity that can be added trivially. In principle, it is possible to find approximation directly by using (1.2), but the result would not conserve momentum and for this reason is seldom used. Following Monaghan [13], the numerical scheme can be improved by first writing

$$\begin{aligned} \dot{\rho} &= -\operatorname{div}(\rho \boldsymbol{v}) + \nabla\rho \cdot \boldsymbol{v}, \\ \dot{\boldsymbol{v}} &= -\nabla\left(\frac{p}{\rho}\right) + \frac{p}{\rho^2}\nabla\rho. \end{aligned} \tag{1.12}$$

Only then, we use (1.2) to obtain

$$\begin{aligned} \dot{\rho}_a &= \sum_b m_b(\boldsymbol{v}_a - \boldsymbol{v}_b) \cdot \nabla W_{h,ab} \\ \dot{\boldsymbol{v}}_a &= -\sum_b m_b \left(\frac{p_a}{\rho_a^2} + \frac{p_b}{\rho_b^2}\right) \nabla W_{h,ab} \end{aligned} \tag{1.13}$$

Note that the equation for ρ can be integrated:

$$\rho_a = C_a + \sum_b m_b W_{h,ab}. \tag{1.14}$$

Constant C_a is determined by initial condition. (For periodic problems, C_a can be set zero. Non-zero value can be used for free surface flows to guarantee stress-free initial state [14, 6].)

The system is closed through a relationship $p = p(\rho)$, which is material specific. For example, in water, the Tait equation [15] can be used

$$p = \frac{\rho_0 c^2}{7}\left(\left(\frac{\rho}{\rho_0}\right)^7 - 1\right) \tag{1.15}$$

where c is the speed of sound and ρ_0 density of referential state. When compression is not large, the linearized formula

$$p = c^2(\rho - \rho_0) \tag{1.16}$$

offers reasonable approximation [16].

Using (1.4), we see that the linear momentum is conserved:

$$\frac{\mathrm{d}}{\mathrm{d}t}\sum_a m_a \boldsymbol{v}_a = \sum_a m_a \dot{\boldsymbol{v}}_a = -\sum_{a,b} m_a m_b \left(\frac{p_a}{\rho_a^2} + \frac{p_b}{\rho_b^2}\right)\nabla W_{h,ab} = 0. \tag{1.17}$$

It is equally simple to demonstrate conservation of angular momentum:

$$\begin{aligned}\frac{\mathrm{d}}{\mathrm{d}t}\sum_a m_a \boldsymbol{x}_a \times \boldsymbol{v}_a &= -\sum_{a,b} m_a m_b \left(\frac{p_a}{\rho_a^2} + \frac{p_b}{\rho_b^2}\right)\boldsymbol{x}_a \times \nabla W_{h,ab} \\ &= -\frac{1}{2}\sum_{a,b} m_a m_b \left(\frac{p_a}{\rho_a^2} + \frac{p_b}{\rho_b^2}\right)(\boldsymbol{x}_a - \boldsymbol{x}_b) \times \nabla W_{h,ab} \\ &= 0,\end{aligned} \tag{1.18}$$

since $\nabla W_{h,ab}$ and $\boldsymbol{x}_a - \boldsymbol{x}_b$ are parallel vectors. To verify conservation energy, we need to find the time derivative of

$$E = \sum_a m_a e_a, \tag{1.19}$$

where e is the specific energy, which satisfies $\frac{\partial e}{\partial \boldsymbol{v}} = \boldsymbol{v}$ and $\frac{\partial e}{\partial \rho} = \frac{p}{\rho^2}$. A simple computation yields:

$$\begin{aligned}\frac{\mathrm{d}E}{\mathrm{d}t} =& \sum_a m_a \left(\boldsymbol{v}_a \cdot \dot{\boldsymbol{v}}_{\boldsymbol{a}} + \frac{p_a}{\rho_a^2}\dot{\rho}_a\right) \\ =& -\sum_{a,b} m_a m_b \left(\frac{p_a}{\rho_a^2} + \frac{p_b}{\rho_b^2}\right)\boldsymbol{v}_a \cdot \nabla W_{h,ab} \\ &+ \sum_{a,b} m_a m_b \frac{p_a}{\rho_a^2}(\boldsymbol{v}_a - \boldsymbol{v}_b)\cdot \nabla W_{h,ab} \\ =& 0\end{aligned} \tag{1.20}$$

because the two sums cancel each other.

As a remark, for arbitrary $f_a = f(\rho_a, \boldsymbol{v}_a)$, we find

$$\frac{\mathrm{d}}{\mathrm{d}t}\sum_a m_a f_a = \sum_a m_a \rho_a \left(\frac{\partial e_a}{\partial \rho_a}\,\mathrm{div}_a\left\{\frac{\partial f}{\partial \boldsymbol{v}}\right\} - \frac{\partial f_a}{\partial \rho_a}\,\mathrm{div}_a\left\{\frac{\partial e}{\partial \boldsymbol{v}}\right\}\right), \tag{1.21}$$

where we defined an SPH divergence operator:

$$\mathrm{div}_a\{\boldsymbol{\varphi}\} = -\frac{1}{\rho_a}\sum_b m_b(\boldsymbol{\varphi}_a - \boldsymbol{\varphi}_b)\cdot \nabla W_{h,ab}. \tag{1.22}$$

Equation (1.21) is, in fact, an equivalent formulation of (1.13), An advantage of this alternative formulation is that the energy conservation becomes a trivial consequence of anti-symmetry of the bilinear form with arguments f, e. Equation

(1.21) can be also understood as a discretization of the fluidic Poisson bracket [17]:

$$\left\{\int f\rho \,\mathrm{d}\boldsymbol{x}, \int e\rho \,\mathrm{d}\boldsymbol{x}\right\} = \int \rho^2 \left(\frac{\partial e}{\partial \rho}\,\mathrm{div}\,\frac{\partial f}{\partial \boldsymbol{v}} - \frac{\partial f}{\partial \rho}\,\mathrm{div}\,\frac{\partial e}{\partial \boldsymbol{v}}\right)\mathrm{d}\boldsymbol{x}. \tag{1.23}$$

We will use the idea later for deriving conservative particle approximations for the symmetric hyperbolic thermodynamically compatible (SHTC) model and also for the Landau-Tizsa model of superfluid helium.

1.3 Convergence analysis

This section is devoted to selected results regarding the convergence of SPH method. It should be said in advance that error estimates derived in this section are very pessimistic and useless from the quantitative point of view (and applicable for periodic domains, which is not the type of problem where SPH could outshine mesh-based approaches). First, we study the continuous interpolation error (also called kernel approximation error), which comes from replacing f with $f * W_h$. Following [12], we can formulate a consistency theorem:

Theorem 1. *Let $f \in C^2(\mathbb{R}^3)$. Then*

$$|f * W_h(\boldsymbol{x}) - f(\boldsymbol{x})| \leq Ch^2 \|\nabla^2 f\|_\infty, \tag{1.24}$$

where constant C depends on the kernel and the dimension (but not on f or h).

Proof. Using Taylor's theorem, we find

$$\begin{aligned} &f * W_h(\boldsymbol{x}) - f(\boldsymbol{x}) \\ &= \int (f(\boldsymbol{y}) - f(\boldsymbol{x})) W_h(\boldsymbol{x} - \boldsymbol{y}) \,\mathrm{d}\boldsymbol{y} \\ &= \int \nabla f(\boldsymbol{x}) \cdot (\boldsymbol{y} - \boldsymbol{x}) W_h(\boldsymbol{x} - \boldsymbol{y}) \,\mathrm{d}\boldsymbol{y} \\ &+ \int \int_0^1 (1-\theta) \nabla^2 f(\boldsymbol{x} + \theta(\boldsymbol{y} - \boldsymbol{x})) : (\boldsymbol{y} - \boldsymbol{x}) \otimes (\boldsymbol{y} - \boldsymbol{x}) W_h(\boldsymbol{x} - \boldsymbol{y}) \,\mathrm{d}\theta \,\mathrm{d}\boldsymbol{y} \end{aligned} \tag{1.25}$$

The term with $\nabla f(\boldsymbol{x})$ vanishes due to the even symmetry of $W_h(\boldsymbol{x} - \boldsymbol{y})$. The sought result follows with constant

$$C = \frac{1}{2} \int \left|\frac{\boldsymbol{x}}{h}\right|^2 W_h(\boldsymbol{x}) \,\mathrm{d}\boldsymbol{x} = \frac{1}{2} \int |\hat{\boldsymbol{x}}|^2 W_1(\hat{\boldsymbol{x}}) \,\mathrm{d}\hat{\boldsymbol{x}}\,. \tag{1.26}$$

□

As a remark, the same estimate can be used on a function $f \in C^3(\Omega)$, which yields

$$|f * \partial_i W_h(\boldsymbol{x}) - \partial_i f(\boldsymbol{x})| \leq Ch^2 \|\nabla^3 f\|_\infty. \tag{1.27}$$

Let us now turn attention to the error of particle approximation introduced by numerical integration:

$$\int f\rho \,\mathrm{d}\boldsymbol{x} \approx \sum_a m_a f(\boldsymbol{x}_a). \tag{1.28}$$

A direct error estimation leads to difficulties because the accuracy will depend on particle arrangement of which we have no prior information. An elegant approach was conceived by Di Lisio[18], who estimates the error from certain regularized fluid equations. We will follow the same approach here. For simplicity, we will restrict ourselves to isentropic inviscid fluid. Treatments of Navier-Stokes equations can be found in literature [19]. To motivate the regularized form of fluid equations, let us begin by writing the hydrodynamic Lagrangian:

$$\mathcal{L}(\chi) = \int \rho_0 \left(\frac{1}{2} |\partial_t \chi|^2 - \epsilon(\rho) \right) \mathrm{d}\boldsymbol{X} \,, \tag{1.29}$$

where $\boldsymbol{X}$ is the reference coordinate, χ is the deformation mapping, ϵ is the specific internal energy and $\rho_0 = \rho_0(\boldsymbol{X})$ is the density in the reference configuration which we take equal to the initial frame. We remind that density in the current configuration can be computed from

$$\rho(\chi(t, \boldsymbol{X})) = \frac{\rho_0(\boldsymbol{X})}{\det\left(\nabla \chi(t, \boldsymbol{X})\right)}. \tag{1.30}$$

To avoid any technicalities with the boundary conditions, we assume fluid in a periodic box (a three-dimensional torus) $\mathbb{T}$, where the period is more that two times larger than the support of kernel W_h. Let us approximate the functional $\mathcal{L}$ by replacing ρ with $\rho_h = \rho * W_h$ in the evaluation of internal energy (attenuating high frequency waves of density):

$$\mathcal{L}_h(\chi) := \int \left(\frac{1}{2} |\partial_t \chi|^2 - \epsilon(\rho_h) \right) M \, \mathrm{d}\mu_0 \left(\boldsymbol{X} \right), \tag{1.31}$$

where $\mathrm{d}\mu_t = \frac{1}{M} \rho \, \mathrm{d}\boldsymbol{X}$ is a probability measure and M is the total mass of the fluid sample. (By conservation of mass, M is constant in time). Density ρ can be recovered from μ as a Radon–Nikodym derivative provided that μ is absolutely continuous with respect to Lebesgue measure.

By the integral substitution theorem, μ_t is a push-forward measure induced from μ_0 by the map $\chi_t = \chi(t, \cdot)$, which fact we denote as $\mu_t = \chi_t \sharp \mu_0$. With an abuse of notation, we can write

$$\rho_h(\mu_t, \boldsymbol{x}) = \int W_h(\boldsymbol{x}, \boldsymbol{y}) M \, \mathrm{d}\mu_t \left(\boldsymbol{y} \right), \tag{1.32}$$

where $W_h(\boldsymbol{x}, \boldsymbol{y})$ is the smoothing kernel evaluated for $r(\boldsymbol{x}, \boldsymbol{y})$, the distance of points $\boldsymbol{x}$ and $\boldsymbol{y}$ in $\mathbb{T}$. The distance $r(\boldsymbol{x}, \boldsymbol{y})$ can be smaller than $|\boldsymbol{x} - \boldsymbol{y}|$ due to periodicity. Alternatively, we can write

$$\rho_h(\mu_t, \boldsymbol{x}) = \int W_h(|\boldsymbol{x} - \boldsymbol{y}|) M \, \mathrm{d}\overline{\mu}_t \left(\boldsymbol{y} \right), \tag{1.33}$$

where $\overline{\mu}$ is a periodic extension of measure μ. Formally minimizing the action of

the Lagrangian over $[0,T]$ with respect to end-point fixing variations $\delta\chi$, we find

$$\begin{aligned}
0 &= \int_0^T \delta\mathcal{L}_h = \int_0^T \int \partial_t\chi(t,\boldsymbol{X})\cdot\partial_t\delta\chi(t,\boldsymbol{X})M\mathrm{d}\mu_0(\boldsymbol{X}) \\
&- \int_0^T \int \epsilon'(\rho_h(\mu_t,\chi(t,\boldsymbol{X})))\delta\rho_h(\mu_t,\chi(t,\boldsymbol{X}))M\mathrm{d}\mu_0(\boldsymbol{X}) \\
&= -\int_0^T \int \partial_{tt}\chi(t,\boldsymbol{X})\cdot\delta\chi(t,\boldsymbol{X})\ M\mathrm{d}\mu_0(\boldsymbol{X})\,\mathrm{d}t \\
&- \int_0^T \int\int \nabla W_h(\chi(t,\boldsymbol{X}),\chi(t,\boldsymbol{Y}))\cdot\delta\chi(t,\boldsymbol{X})\epsilon'(\rho_h(\mu_t,\chi(t,\boldsymbol{X})))M^2\mathrm{d}\mu_0^2(\boldsymbol{X},\boldsymbol{Y})\,\mathrm{d}t \\
&+ \int_0^T \int\int \nabla W_h(\chi(t,\boldsymbol{X}),\chi(t,\boldsymbol{Y}))\cdot\delta\chi(t,\boldsymbol{Y})\epsilon'(\rho_h(\mu_t,\chi(t,\boldsymbol{X})))M^2\mathrm{d}\mu_0^2(\boldsymbol{X},\boldsymbol{Y})\,\mathrm{d}t \\
&= -\int_0^T \int \Big[\partial_{tt}\chi - \boldsymbol{F}_h(\mu_t,\phi(t,\boldsymbol{X}))\Big]\cdot\delta\chi(t,\boldsymbol{X})M\,\mathrm{d}\mu_0\,(\boldsymbol{X}),
\end{aligned} \tag{1.34}$$

where ∇W is the gradient of $W(\cdot,\cdot)$ with respect to first component and (since $\epsilon' = \frac{p}{\rho^2}$)

$$\boldsymbol{F}_h(\mu_t,\boldsymbol{x}) = -\int \left(\frac{p(\rho_h(\mu_t,\boldsymbol{y}))}{\rho_h^2(t,\boldsymbol{y})} + \frac{p(\rho_h(\mu_t,\boldsymbol{x}))}{\rho_h^2(t,\boldsymbol{x})}\right)\nabla W_h(\boldsymbol{x},\boldsymbol{y})M\,\mathrm{d}\mu_t\,(\boldsymbol{y}), \tag{1.35}$$

for any $\delta\chi$ with fixed endpoints. Note that $\boldsymbol{F}_h$ remains well-defined when χ is not one-to-one or $\nabla\chi$ is singular. In other words, we can relax the assumption that μ_t is absolutely continuous and ρ exists as a function. A convenient tool in SPH theory is the Wasserstein metric:

Definition 1. *Symbol $P(\mathbb{T})$ will denote the space of all Radon probability measures in $\mathbb{T}$. For $\mu,\nu\in\mathcal{P}(\mathbb{T})$, we say that probability measure P on $\mathbb{T}\times\mathbb{T}$ is a joint distribution with marginals μ,ν if*

$$\begin{aligned}
\int\int \varphi(\boldsymbol{x})\,\mathrm{d}P\,(\boldsymbol{x},\boldsymbol{y}) &= \int\int \varphi(\boldsymbol{x})\,\mathrm{d}\mu\,(\boldsymbol{x}), \\
\int\int \varphi(\boldsymbol{y})\,\mathrm{d}P\,(\boldsymbol{x},\boldsymbol{y}) &= \int\int \varphi(\boldsymbol{y})\,\mathrm{d}\nu\,(\boldsymbol{x}),
\end{aligned} \tag{1.36}$$

for any integrable φ. The Wasserstein distance of measures μ,ν is

$$\mathcal{W}(\mu,\nu) = \inf_P \int\int r(\boldsymbol{x},\boldsymbol{y})\,\mathrm{d}P\,(\boldsymbol{x},\boldsymbol{y}), \tag{1.37}$$

where the infimum is taken over all joint distributions with marginals μ,ν.

The Wasserstein metric is sometimes referred to as *earth-mover distance*. When density functions of μ,ν are interpreted as elevations before and after land transformation and $\mathrm{d}P\,(\boldsymbol{x},\boldsymbol{y})$ is a measure of soil moved from $\boldsymbol{x}$ to $\boldsymbol{y}$, then $\mathcal{W}$ is proportional to the least work required for the said terrain change. The space $\mathcal{P}(\mathbb{T})$ is complete when equipped with the Wasserstein metric [20]. We are led to the following definition[1]:

[1] $C^{0,1}$ denotes Lipschitz continuous functions.

Definition 2. *For given initial data $\boldsymbol{V} \in C^{0,1}(\mathbb{T}, \mathbb{R}^3)$ and $\mu_0 \in \mathcal{P}(\mathbb{T})$, we say that functions $\chi \in C^2(0,T; C^{0,1}(\mathbb{T}, \mathbb{R}^3))$ and $\mu \in C(0,T; \mathcal{P}(\mathbb{T}))$ are solutions of the regularized Euler system if, for every $t \in [0,T]$:*

$$\begin{aligned} &\partial_{tt}\chi(t, \boldsymbol{X}) = \boldsymbol{F}_h(\mu_t, \chi(t, \boldsymbol{X})), \\ &\mu_t = \chi_t \sharp \mu_0, \\ &\chi(0, \boldsymbol{X}) = \boldsymbol{X}, \\ &\partial_t \chi(0, \boldsymbol{X}) = \boldsymbol{V}(\boldsymbol{X}). \end{aligned} \tag{1.38}$$

This integro-differential equation is a Hamiltonian, regularized version of Euler fluid equations and has nice properties, like global existence of solution. Before we can proceed with existence proof, we make the assumption that internal energy ϵ is $C^2[0,\infty)$ as a function of ρ. It is feasible to allow singularity for $\rho \to 0^+$, but the proof would be more technical and only local in time. We begin the proof with a crucial lemma:

Lemma 2. *For any fixed $h > 0$, there are constants C_1 and C_2 such that:*

$$|\rho_h(\mu, \boldsymbol{x}) - \rho_h(\nu, \boldsymbol{y})| \leq C_1 \left(r(\boldsymbol{x}, \boldsymbol{y}) + \mathcal{W}(\mu, \nu) \right), \tag{1.39}$$

$$|\boldsymbol{F}_h(\mu, \boldsymbol{x}) - \boldsymbol{F}_h(\nu, \boldsymbol{y})| \leq C_2 \left(r(\boldsymbol{x}, \boldsymbol{y}) + \mathcal{W}(\mu, \nu) \right). \tag{1.40}$$

Proof. As a first observation, we have an upper bound for density:

$$\rho_h(\mu, \boldsymbol{x}) = \int W_h(\boldsymbol{x}, \boldsymbol{y}) M \, \mathrm{d}\mu_t(\boldsymbol{y}) \leq M \|W_h\|_\infty =: \rho_{h,\max}. \tag{1.41}$$

Let $\|\epsilon'\|_\infty$ and $\|\epsilon''\|_\infty$ be the bound and Lipschitz constant of $\epsilon' = \frac{p}{\rho^2}$ respectively on interval $[0, \rho_{h,\max}]$. First, we analyze the special case $\mu = \nu$.

$$\begin{aligned} |\rho_h(\mu, \boldsymbol{x}) - \rho_h(\mu, \boldsymbol{y})| &\leq M \int |W(\boldsymbol{x}, \boldsymbol{z}) - W(\boldsymbol{y}, \boldsymbol{z})| \, \mathrm{d}\mu(\boldsymbol{z}) \\ &\leq M \|\nabla W_h\|_\infty r(\boldsymbol{x}, \boldsymbol{y}) \end{aligned} \tag{1.42}$$

and

$$\begin{aligned} &|\boldsymbol{F}_h(\mu, \boldsymbol{x}) - \boldsymbol{F}_h(\mu, \boldsymbol{y})| \leq M \int \left| \epsilon'(\rho_h(\mu, \boldsymbol{x})) - \epsilon'(\rho_h(\mu, \boldsymbol{y}) \right| \left| \nabla W_h(\boldsymbol{x}, \boldsymbol{z}) \right| \mathrm{d}\mu(\boldsymbol{z}) \\ &+ M \int \left| \epsilon'(\rho_h(\mu, \boldsymbol{y})) + \epsilon'(\rho_h(\mu, \boldsymbol{z})) \right| \left| \nabla W_h(\boldsymbol{x}, \boldsymbol{z}) - \nabla W_h(\boldsymbol{y}, \boldsymbol{z}) \right| \mathrm{d}\mu(\boldsymbol{z}) \\ &\leq \left(M^2 \|\epsilon''\|_\infty \|\nabla W_h\|_\infty^2 + 2M \|\epsilon'\|_\infty \|\nabla^2 W_h\|_\infty \right) r(\boldsymbol{x}, \boldsymbol{y}). \end{aligned} \tag{1.43}$$

Next, we consider $\boldsymbol{x} = \boldsymbol{y}$ but different μ, ν. Let P be any joint distribution with marginals μ, ν. Then

$$\begin{aligned} |\rho_h(\mu, \boldsymbol{x}) - \rho_h(\nu, \boldsymbol{x})| &\leq M \int \int \left| W_h(\boldsymbol{x}, \boldsymbol{y}) - W_h(\boldsymbol{x}, \boldsymbol{z}) \right| \mathrm{d}P(\boldsymbol{y}, \boldsymbol{z}) \\ &\leq M \|\nabla W_h\|_\infty \int \int r(\boldsymbol{y}, \boldsymbol{z}) \, \mathrm{d}P(\boldsymbol{y}, \boldsymbol{z}). \end{aligned} \tag{1.44}$$

Minimizing over P, we find:

$$|\rho_h(\mu, \boldsymbol{x}) - \rho_h(\nu, \boldsymbol{x})| \leq M \|\nabla W_h\|_\infty \mathcal{W}(\mu, \nu). \tag{1.45}$$

Estimate for F_h is analogous:

$$\begin{aligned}
&\boldsymbol{F}_h(\mu, \boldsymbol{x}) - \boldsymbol{F}_h(\nu, \boldsymbol{x}) = \\
&- M \int \left[\epsilon'(\mu, \boldsymbol{x}) + \epsilon'(\mu, \boldsymbol{y}) - \epsilon'(\nu, \boldsymbol{x}) - \epsilon'(\nu, \boldsymbol{y}) \right] \nabla W_h(\boldsymbol{x}, \boldsymbol{y}) \, \mathrm{d}\mu \, (\boldsymbol{y}) \\
&- M \int \left[\epsilon'(\nu, \boldsymbol{x}) + \epsilon'(\nu, \boldsymbol{y}) \right] \nabla W_h(\boldsymbol{x}, \boldsymbol{y}) \, \mathrm{d}(\mu - \nu) \, (\boldsymbol{y}) \\
&= I_1 + I_2.
\end{aligned} \tag{1.46}$$

Integral I_1 can be easily estimated using Lipschitz continuity of ϵ' and (1.45):

$$|I_1| \leq 2M^2 \|\epsilon''\|_\infty \|\nabla W\|_\infty^2 \mathcal{W}(\mu, \nu). \tag{1.47}$$

Again, let P be joint distribution with marginals μ, ν. We expand integral I_2:

$$\begin{aligned}
I_2 &= -M \int \int \left[\epsilon'(\mu, \boldsymbol{x}) + \epsilon'(\mu, \boldsymbol{y}) \right] \Big(\nabla W_h(\boldsymbol{x}, \boldsymbol{y}) - \nabla W_h(\boldsymbol{x}, \boldsymbol{z}) \Big) \, \mathrm{d}P \, (\boldsymbol{y}, \boldsymbol{z}) \\
&- M \int \int \left[\epsilon'(\mu, \boldsymbol{y}) - \epsilon'(\mu, \boldsymbol{z}) \right] \nabla W_h(\boldsymbol{x}, \boldsymbol{z}) \, \mathrm{d}P \, (\boldsymbol{y}, \boldsymbol{z}) \\
&= I_{2a} + I_{2b},
\end{aligned} \tag{1.48}$$

where

$$|I_{2a}| \leq 2M \|\epsilon'\|_\infty \|\nabla^2 W_h\|_\infty \int \int r(\boldsymbol{y}, \boldsymbol{z}) \, \mathrm{d}P \, (\boldsymbol{y}, \boldsymbol{z}) \tag{1.49}$$

and, using (1.42),

$$|I_{2b}| \leq M^2 \|\epsilon''\|_\infty \|\nabla W_h\|_\infty^2 \int \int r(\boldsymbol{y}, \boldsymbol{z}) \, \mathrm{d}P \, (\boldsymbol{y}, \boldsymbol{z}). \tag{1.50}$$

Minimizing over P leads to the sought result. □

Theorem 3. *Solutions of the regularized Euler system exist and are unique.*

Proof. Let S be the space of all $\nu \in C(0, T; \mathcal{P}(\mathbb{T}))$, such that $\nu_0 = \mu_0$. Using standard theory, we see that for every fixed $\nu \in S$ and $\boldsymbol{X} \in \mathbb{T}$, there is unique $\chi(\cdot, \boldsymbol{X}) \in C^2$, which solves an ordinary differential equation:

$$\begin{aligned}
&\partial_{tt} \chi(t, \boldsymbol{X}) = \boldsymbol{F}_h(\nu_t, \chi(t, \boldsymbol{X})), \\
&\chi(0, \boldsymbol{X}) = \boldsymbol{X}, \\
&\partial_t \chi(0, \boldsymbol{X}) = \boldsymbol{V}(\boldsymbol{X}),
\end{aligned} \tag{1.51}$$

since the right-hand side is globally Lipschitz continuous by Lemma 2. Set $\mu_t = \chi_t \sharp \mu_0$. It suffices to show that the mapping $\Theta : \nu \mapsto \mu$ defines a contraction in S. To this end, let $\tilde{\nu} \in S$, $\tilde{\mu} = \Theta(\tilde{\nu})$ and $\tilde{\chi}$ be the corresponding solution of (1.51). Using the differential equation and Lemma 2, we can estimate:

$$\begin{aligned}
&r(\chi(t, \boldsymbol{X}), \tilde{\chi}(t, \boldsymbol{Y})) \leq r(\boldsymbol{X}, \boldsymbol{Y}) + \int_0^t |\partial_t \chi(s, \boldsymbol{X}) - \partial_t \tilde{\chi}(s, \boldsymbol{Y})| \, \mathrm{d}s \\
&\leq r(\boldsymbol{X}, \boldsymbol{Y}) + t|V(\boldsymbol{X}) - V(\boldsymbol{Y})| + \int_0^t \int_0^s \Big| \boldsymbol{F}_h(\mu_\tau, \chi(\tau, \boldsymbol{X})) - \boldsymbol{F}_h(\tilde{\mu}_\tau, \tilde{\chi}(\tau, \boldsymbol{Y})) \Big| \mathrm{d}\tau \mathrm{d}s \\
&\leq r(\boldsymbol{X}, \boldsymbol{Y})(1 + tL_{\boldsymbol{V}}) + C_2 \int_0^t (t - \tau) \Big[r(\chi(\tau, \boldsymbol{X}), \tilde{\chi}(\tau, \boldsymbol{Y})) + \mathcal{W}(\mu_\tau, \tilde{\mu}_\tau) \Big] \, \mathrm{d}\tau \, ,
\end{aligned} \tag{1.52}$$

where $L_{\boldsymbol{V}}$ is a Lipschitz constant of V. A joint distribution P_t with marginals $\mu_t, \tilde{\mu}_t$ can be defined such that

$$\int\int f(\boldsymbol{x},\boldsymbol{y})\,\mathrm{d}P_t(\boldsymbol{x},\boldsymbol{y}) = \int f(\chi(t,\boldsymbol{X}),\tilde{\chi}(t,\boldsymbol{X}))\,\mathrm{d}\mu_0(\boldsymbol{X}), \tag{1.53}$$

for any integrable function f. Combining (1.52) (with $X = Y$) and (1.53), we infer

$$\begin{aligned} R(t) &:= \int\int r(\boldsymbol{x},\boldsymbol{y})\,\mathrm{d}P_t\,(\boldsymbol{x},\boldsymbol{y}) \\ &= \int r(\chi(t,\boldsymbol{X}),\tilde{\chi}(t,\boldsymbol{X}))\,\mathrm{d}\mu_0\,(\boldsymbol{X}) \\ &\leq C_2T^2 \sup_{s\in[0,T]} \mathcal{W}(\nu_s,\tilde{\nu}_s) + C_2\int_0^t (t-\tau)R(\tau)\,\mathrm{d}\tau \end{aligned} \tag{1.54}$$

and, using the integral form of Grönwall inequality,

$$\mathcal{W}(\mu_t,\tilde{\mu}_t) \leq R(t) \leq C_2T^2e^{C_2T^2} \sup_{s\in[0,T]} \mathcal{W}(\nu_s,\tilde{\nu}_s), \quad \forall t\in[0,T] \tag{1.55}$$

This proves that Θ is a contraction for sufficiently small T and demonstrates local existence and uniqueness by Banach fixed-point theorem. In other words, the solution provably exists on a time interval $[0,\Delta t]$, for some small Δt. Note that Δt depends only on C_2 and not on $\boldsymbol{V}$ or μ_0. The solution can be then extended to $[0,T]$ by partitioning the interval into time steps smaller than Δt, and repeating the contraction argument above.

It remains to show that χ is Lipschitz continuous with respect to spatial variable $\boldsymbol{X}$. From (1.52), if follows that for $\boldsymbol{X} \neq \boldsymbol{Y}$:

$$\frac{r(\chi(t,\boldsymbol{X}),\chi(t,\boldsymbol{Y}))}{r(\boldsymbol{X},\boldsymbol{Y})} \leq 1 + tL_{\boldsymbol{V}} + C_2\int_0^t (t-\tau)\frac{r(\chi(\tau,\boldsymbol{X}),\chi(\tau,\boldsymbol{Y}))}{r(\boldsymbol{X},\boldsymbol{Y})}\,\mathrm{d}\tau\,. \tag{1.56}$$

The sought result is obtained by another application of Grönwall inequality. □

Now, SPH corresponds exactly to the solution of regularized Euler system for a special initial condition:

Theorem 4. *Suppose that* $\boldsymbol{V} \in C^1(\mathbb{T},\mathbb{R}^3)$ *and*

$$\mu_0 = \frac{1}{M}\sum_a m_a\delta_{\boldsymbol{X}_a}. \tag{1.57}$$

Let $\boldsymbol{x}_a, a = 1,\dots N$ *be SPH solution of* (1.13) *with initial condition*

$$\begin{aligned} \boldsymbol{x}_a(0) &= \boldsymbol{X}_a, \\ \boldsymbol{v}_a(0) &= \boldsymbol{V}(\boldsymbol{X}_a), \\ \rho_a(0) &= \mu_0 * W_h(\boldsymbol{X}_a). \end{aligned} \tag{1.58}$$

Then, the solution (χ,μ) *of regularized Euler system satisfies*

$$\begin{aligned} \boldsymbol{x}_a(t) &= \chi(t,\boldsymbol{X}_a), \\ \mu_t &= \frac{1}{M}\sum_a m_a\delta_{\boldsymbol{x}_a(t)}. \end{aligned} \tag{1.59}$$

for every $t\in[0,T]$.

Proof. By definition of μ_t, we know that

$$\mu_t = \chi_t \sharp \mu_0 = \frac{1}{M} \sum_a m_a \delta_{\chi(t, \boldsymbol{X}_a)} \tag{1.60}$$

and thus

$$\rho_h(\mu_t, \boldsymbol{x}_a) = \int W_h(\boldsymbol{x}, \boldsymbol{y}) M \mathrm{d}\mu_t(\boldsymbol{y}) = \sum_b m_b W_h(\boldsymbol{x}_a, \boldsymbol{x}_b) = \rho_a \tag{1.61}$$

and

$$\boldsymbol{F}_h(\mu_t, \boldsymbol{x}_a) = -\sum_b m_b \left(\frac{p(\rho_a)}{\rho_a^2} + \frac{p(\rho_b)}{\rho_b^2} \right) \nabla W_h(\boldsymbol{x}_a, \boldsymbol{x}_b) \tag{1.62}$$

The proof then follows since $\boldsymbol{x}_a(t)$ and $\chi(t, \boldsymbol{X}_a)$ solve exactly the same system of differential equations with unique solution. □

Naturally, we ask whether the discrete initial condition μ_0^N of SPH method approaches the smooth initial condition $\mathrm{d}\mu_0 = \rho_0 \, \mathrm{d}\boldsymbol{x}$ in Wasserstein metric. The answer is affirmative.

Theorem 5. *Let $\mu_0 \in \mathcal{P}(\mathbb{T})$ and suppose that $\mathbb{T}$ is covered by N cells $C_a, a = 1, \ldots, N$ such that $\mu_0(C_a \cap C_b) = 0$ whenever $a \neq b$ and each cell C_a is a subset of a ball with center $\boldsymbol{X}_a$ and radius δr. Then*

$$\mathcal{W}(\mu_0, \mu_0^N) \leq \delta r, \tag{1.63}$$

where

$$\begin{aligned} \mu_0^N &= \frac{1}{M} \sum_a m_a \delta_{\boldsymbol{X}_a}, \\ m_a &= M \int_{C_a} \mathrm{d}\mu_0 \, (\boldsymbol{X}). \end{aligned} \tag{1.64}$$

Proof. Consider a joint representation P_0 of (μ_0, μ_0^N) given by

$$\int \int f(\boldsymbol{X}, \boldsymbol{Y}) \mathrm{d}P_0(\boldsymbol{X}, \boldsymbol{Y}) = \sum_a \int_{C_a} f(\boldsymbol{X}, \boldsymbol{X}_a) \, \mathrm{d}\mu_0 \, (\boldsymbol{X}). \tag{1.65}$$

From here, we can estimate

$$\mathcal{W}(\mu_0, \mu_0^N) \leq \int \int r(\boldsymbol{X}, \boldsymbol{Y}) \mathrm{d}P_0(\boldsymbol{X}, \boldsymbol{Y}) = \sum_a \int_{C_a} r(\boldsymbol{X}, \boldsymbol{X}_a) \, \mathrm{d}\mu_0 \, (\boldsymbol{X}) \leq \delta r. \tag{1.66}$$

□

The assumptions of theorem 5 are easily satisfied by arranging initial particles in any regular grid (e.g. square or hexagonal grid in two dimensions or any type of cubic grid in three dimensions).

Finally, we are ready to prove that, for fixed h, SPH approximation converges to the solution of regularized Euler equation as $\delta r \to 0$. By Theorems 4 and 5, convergence is effectively reduced to the problem of sensitivity with respect to initial condition.

Theorem 6. *Let (χ, μ) be a solution of regularized Euler equations for some h, T, μ_0 and $\boldsymbol{V}$. Let $\boldsymbol{X}_a$ and m_a satisfy the assumptions of theorem 5 and $\boldsymbol{x}_a = \boldsymbol{x}_a(t)$ be positions of smoothed particles with initial condition $\boldsymbol{x}_a(0) = \boldsymbol{X}_a$ and with $\dot{\boldsymbol{x}}_a(0) = \boldsymbol{V}(\boldsymbol{X}_a)$. Then*

$$\sup_{t\in[0,T]} \max_a r(\boldsymbol{x}_a(t), \chi(t, \boldsymbol{X}_a)) + \sup_{t\in[0,T]} \mathcal{W}\left(\mu_t, \mu_t^N\right) = O(\delta r), \tag{1.67}$$

where

$$\mu^N(t) = \sum_a \frac{m_a}{M} \delta_{\boldsymbol{x}_a(t)}. \tag{1.68}$$

Proof. Denote (χ^N, μ^N) the solution of regularized Euler equations which is same as (χ, μ) except it is solved for discrete initial mass distribution $\mu^N(0)$. We begin by estimating $\mathcal{W}(\mu_t, \mu_t^N)$. Let P_0 be a joint distribution with marginals μ_0, μ_0^N and P_t a push-forward by $\chi \times \chi^N$. Using (1.52), we find

$$\begin{aligned} r(\chi(t, \boldsymbol{X}), \chi^N(t, \boldsymbol{Y})) &\le (1 + tL_{\boldsymbol{V}}) r(\boldsymbol{X}, \boldsymbol{Y}) \\ &\quad + C_2 \int_0^t (t-\tau) \Big[r(\chi(\tau, \boldsymbol{X}), \chi^N(\tau, \boldsymbol{Y})) + \mathcal{W}(\mu_\tau, \mu_\tau^N) \Big] \, \mathrm{d}\tau \end{aligned} \tag{1.69}$$

Hence

$$\begin{aligned} R(t) &:= \int\int r(\chi(t, \boldsymbol{X}), \chi^N(t, \boldsymbol{Y})) \, \mathrm{d}P_0 \, (\boldsymbol{X}, \boldsymbol{Y}) \\ &\le (1 + tL_{\boldsymbol{V}}) R(0) + 2C_2 \int_0^t (t-\tau) R(\tau) \, \mathrm{d}\tau \end{aligned} \tag{1.70}$$

and by Grönwall inequality:

$$\mathcal{W}(\mu_t, \mu_t^N) \le R(t) \le (1 + TL_{\boldsymbol{V}}) R(0) e^{CT^2}, \qquad t \in [0, T]. \tag{1.71}$$

Taking infimum over P_0 and using theorem 5, we find

$$\sup_{t\in[0,T]} \mathcal{W}(\mu_t, \mu_t^N) = O(\delta r) \tag{1.72}$$

Substituting $\boldsymbol{Y} = \boldsymbol{X}$ in (1.69) gives the estimate for $r(\chi(t, X), \chi^N(t, X))$. A direct application of Theorem 4 finishes the proof. □

Unfortunately, the estimate (1.71) is not very useful because the constant C_2 depends on h unfavorably. To conclude the proof of convergence in the sense of an iterated limit

$$\lim_{h\to 0} \lim_{\delta r \to 0} \tag{1.73}$$

we would also need to show that the solutions of the interpolated system (1.38) converge to solutions of the actual Euler equations for smooth initial data as $h \to 0$ (at least locally in time). This would require h-uniform energy estimates for ρ, v and their derivatives. The proof is done in [21] by studying a suitable seminorm. The technique is similar to the proof of local existence of solutions for a systems of conservation laws [22]. Unfortunately, the study was conducted only for a non-conservative force term:

$$\boldsymbol{F}_h = -\frac{\nabla p(\rho_h)}{\rho_h} \tag{1.74}$$

with a specific choice of $p = p(\rho)$. The convergence proof for conservative kernel approximation seems to be missing in literature.

1.4 Symplectic integrators

With the closed form expression for density (1.14), it is easy to see that the SPH approximation constitutes a discrete Hamiltonian system:

$$\begin{aligned} \dot{\boldsymbol{x}}_a &= \frac{1}{m_a}\frac{\partial E}{\partial \boldsymbol{v}_a}, \\ m_a \dot{\boldsymbol{v}}_a &= -\frac{\partial E}{\partial \boldsymbol{x}_a}, \end{aligned} \tag{1.75}$$

where

$$E = \sum_a m_a \left(\frac{1}{2} v_a^2 + \epsilon(\rho_a)\right). \tag{1.76}$$

For this reason, it is advantageous to use *symplectic integrators* when discretizing time. The main selling point of these integrators is that they conserve certain energy E_h, which is close to the true energy [23]. Since SPH simulations often involve large number of small time steps, this property makes them preferable over other methods, like Runge-Kutta schemes. The most basic first-order example is the *symplectic Euler method*:

$$\begin{aligned} \boldsymbol{v}_a(t_{k+1}) &= \boldsymbol{v}_a(t_k) + \frac{\delta t}{m_a}\, \boldsymbol{f}_a(t_k), \\ \boldsymbol{x}_a(t_{k+1}) &= \boldsymbol{x}_a(t_k) + \delta t\, \boldsymbol{v}_a(t_{k+1}), \end{aligned} \tag{1.77}$$

Here, $\boldsymbol{f}_a(t) = -\frac{\partial E}{\partial \boldsymbol{x}_a}$, which is evaluated for particle coordinates at time t. A slightly more sophisticated example of second order is the Verlet integrator (equivalent to leap-frog scheme):

$$\begin{aligned} \boldsymbol{v}_a(t_{k+\frac{1}{2}}) &= \boldsymbol{v}_a(t_k) + \frac{\delta t}{2m_a}\, \boldsymbol{f}_a(t_k), \\ \boldsymbol{x}_a(t_{k+1}) &= \boldsymbol{x}_a(t_k) + \delta t\, \boldsymbol{v}_a(t_{k+\frac{1}{2}}), \\ \boldsymbol{v}_a(t_{k+1}) &= \boldsymbol{v}_a(t_{k+\frac{1}{2}}) + \frac{\delta t}{2m_a}\, \boldsymbol{f}_a(t_{k+1}) \end{aligned} \tag{1.78}$$

Both of these integrators are explicit and conserve energy $E_h = E + O(\delta t^s)$ for sufficiently small δt, where $s = 1$ for symplectic Euler and $s = 2$ for Verlet [23]. Hence, the energy error does not depend explicitly on t. The energy E_h can be found using Baker-Hausdorff-Campbell formula [23]. Verlet scheme provides increased accuracy without significant impact on computation cost (there is still one force calculation per step). Additionally, it is time reversible, which means that inverting velocities is equivalent to inverting the arrow of time. Since this is a fundamental symmetry of Euler fluid equations (for smooth solutions without shocks, at least), we might want to preserve it in our approximation. It should be said, however, that strict time reversibility requires very careful implementation, which involves using fixed point arithmetic instead of the more usual floating point arithmetic, as investigated in our paper [6]. Even then, irreversible behavior is self-emergent for coarsely sampled quantities in a manner analogical to Kac ring [24].

It must be emphasized that the closed formula for density (1.14) needs to be used instead of the time evolution (1.13). Otherwise, the conservative properties of symplectic integrators are lost.

Third and fourth order symplectic integrators are given by Ruth [25] and Yoshida [26]. But since the spatial approximation of SPH is not that precise, using high order time integrators yields diminishing returns.

1.5 Viscous forces

To obtain particle approximation of Navier-Stokes model, one needs to discretize viscous force term

$$\boldsymbol{f}_{\text{visc}} = 2\mu \boldsymbol{\nabla} \cdot \mathbb{D}, \tag{1.79}$$

where $\mathbb{D} = \frac{1}{2}\left(\nabla \boldsymbol{v} + \nabla \boldsymbol{v}^T\right)$ is the velocity deformation tensor and μ is the shear viscosity. A naive approach is to use a kernel approximation and move two derivatives onto the kernel. However, this approach is not recommended as it involves a second derivative of the smoothing kernel, which is generally ill-behaved [12]. One possible choice is the Morris' operator [27]:

$$\boldsymbol{f}_{\text{visc,h}} = 2\mu \sum_b \frac{m_b}{\rho_b} \frac{W'_{h,ab}}{r_{ab}} \boldsymbol{v}_{ab}, \tag{1.80}$$

where $\boldsymbol{v}_{ab} = \boldsymbol{v}_a - \boldsymbol{v}_b$, $\boldsymbol{x}_{ab} = \boldsymbol{x}_a - \boldsymbol{x}_b$ and $r_{ab} = |\boldsymbol{x}_a - \boldsymbol{x}_b|$. Following Monaghan, we can also employ a discrete operator known in molecular dynamics [28]:

$$\boldsymbol{f}_{\text{visc,h}} = 2(d+2)\mu \sum_b \frac{m_b}{\rho_b} W'_{h,ab} \frac{\boldsymbol{v}_{ab} \cdot \boldsymbol{x}_{ab}}{r_{ab}^2 + \eta^2}. \tag{1.81}$$

where η is a small numerical parameter, which prevents division by zero for overlapping particles, and d is the geometric dimension. The latter operator is usually preferred, as it conserves angular momentum. It is also possible to implement bulk viscosity in SPH [12], but the effect will be minor for weakly compressible flows.

For discretizing equations with fluid viscosity, the natural extension of Verlet scheme puts dissipative step in between the update of particle positions [29].

$$\begin{aligned}
\boldsymbol{v}_a(t_{k+\frac{1}{2}}) &= \boldsymbol{v}_a(t_k) + \frac{\delta t}{2m_a}\, \boldsymbol{f}_a(t_k), \\
\boldsymbol{x}_a(t_{k+\frac{1}{2}}) &= \boldsymbol{x}_a(t_k) + \frac{\delta t}{2}\, \boldsymbol{v}_a(t_{k+\frac{1}{2}}), \\
\tilde{\boldsymbol{v}}_a(t_{k+\frac{1}{2}}) &= \boldsymbol{v}_a(t_{k+\frac{1}{2}}) + \frac{1}{\rho_a} \boldsymbol{f}_{\text{visc,h}}(t_{k+\frac{1}{2}}) \\
\boldsymbol{x}_a(t_{k+1}) &= \boldsymbol{x}_a(t_{k+\frac{1}{2}}) + \frac{\delta t}{2}\, \tilde{\boldsymbol{v}}_a(t_{k+\frac{1}{2}}), \\
\boldsymbol{v}_a(t_{k+1}) &= \tilde{\boldsymbol{v}}_a(t_{k+\frac{1}{2}}) + \frac{\delta t}{2m_a}\, \boldsymbol{f}_a(t_{k+1})
\end{aligned} \tag{1.82}$$

This scheme requires two cell list computations per step.

1.6 Dam break

In this two-dimensional example from [12], classical SPH is illustrated on a collapse of a water column on a dry bed, which can be considered a simplified

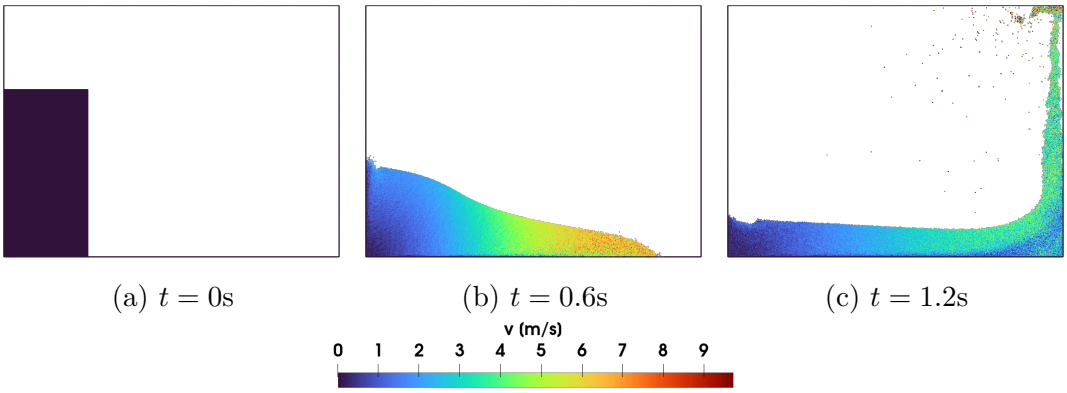

(a) $t = 0$s (b) $t = 0.6$s (c) $t = 1.2$s

Figure 1.2: Snapshots of dam break simulation. Colormap indicates magnitude of velocity.

simulation of dam break. In the initial configuration, fluid is contained inside a rectangle $(0, a) \times (0, 2a)$ in a container of size $(0, 4a) \times (0, 3a)$, where $a = 1$m. The physical parameters are $\rho_0 = 10^3 \text{kg/m}^3$ and $\nu = 10^{-6}\text{m}^2/\text{s}$ and the state equation of Tait (1.15) is used. The gravitational acceleration is $g = 9.8\text{m/s}^2$. The problem involves two different boundary conditions. Firstly, the free surface, which does not require any implementation.[2] Secondly, impenetrable walls (no-slip) need to be modeled. These can be implemented by several layers of dummy particles, which are identical to fluid particles, except their velocity and positions are fixed. For the number of layers, we use

$$n_{\text{layers}} = \left\lceil \frac{2h}{\delta r} \right\rceil . \tag{1.83}$$

Result of the simulation can be seen in figures Fig 1.2 and Fig 1.3. Our numerical result is in a good agreement with available reference solution, although slightly lagging behind the experiment by Koshizuka and Oka due to unknown factors.

[2]To understand this, imagine there are two types of particles in (1.13), some of which belong to air. Air particles will be about 1000 times lighter than water particles. In the approximation $m_{\text{air}}/m_{\text{water}} \to 0$, the air particles have no effect on the dynamics of water as if they were absent in the simulation. Note this argument would fail without the Monaghan's trick (1.12).

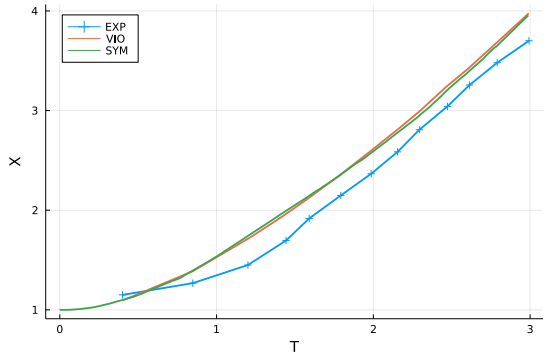

Figure 1.3: Plot of $X = x_{\text{wave}}/a$, where x_{wave} is the x-coordinate of wavefront with respect to dimensionless time $T = t/\sqrt{2ga}$. Comparison of a symplectic simulation (SYM) made with our publicly available *SmoothedParticles.jl* library, the numerical result from Violeau's book (VIO) and an experimental measurement (EXP) [30].

2. SPH for SHTC model

The symmetric hyperbolic thermodynamically compatible (SHTC) model (sometimes called GPR model after Godunov, Peshkov and Romensky) is a unified Eulerian description for fluids and solids [31]. In SHTC, material is described with an additional matrix variable called *distortion field* $\mathbb{A}$, which contributes to the internal energy. For elastic materials, $\mathbb{A}$ is equal to the inverse of deformation $\mathbb{F} = \nabla\chi$, where χ is the map from reference to current configuration. Fluidity is introduced through a relaxation term, which drives $\mathbb{A}$ towards orthogonal matrices. The rate of this irreversible force is inversely proportional to *relaxation time*, denoted τ. The relaxation time measures, loosely speaking, how quickly bonds between molecules rearrange after shear deformation [32]. When $\tau = \infty$, there is no relaxation and SHTC describes an elastic solid. Material similar to Navier-Stokes fluid is obtained when τ is small in comparison to simulation time. The limit $\tau \to 0$ leads to infinitel;y stiff relaxation, which is effectively an orthogonality constraint of $\mathbb{A}$.This corresponds to inviscid fluid. Large τ is similar to Maxwell's viscoelastic fluid. Bingham fluids and plastic solids can be achieved through stress-dependent relaxation time [33]. As shown in [34], SHTC is also compatible with the natural configuration framework, where $\mathbb{A}$ describes the mapping from the current configuration to the natural one.

The ability to seamlessly describe fluids, solids (and anything between) makes SHTC attractive for problems with multiphase flows, especially those with phase change (additive manufacturing, ice formation, land slides, etc.). Another feature of the model is hyperbolicity, which guarantees finite speed of information. For example, an impulse of shear flow in a viscous fluid described by SHTC model will generate waves which move at shear sound speed c_{shear}. This is unlike the Navier-Stokes model, where the response is felt instantaneously for arbitrary large distances. For very short time scales $t \ll \tau$, the SHTC fluid behaves always like an elastic solid. A theoretical disadvantage of SHTC is that, due to absence of parabolic terms, existence of solutions can be proven only locally in time [35].

2.1 Derivation from Poisson brackets

Now, let us show how reversible part of SHTC model can be derived from Poisson brackets. The following derivation will be only formal, lacking mathematical rigor. However, the procedure will be useful tool for finding a conservative particle approximation. We begin by writing the canonical Poisson bracket in continuum [17] (see also Appendix A):

$$\{U, E\} = \int \left(\frac{\delta U}{\delta \chi_i} \frac{\delta E}{\delta M_i} - \frac{\delta E}{\delta \chi_i} \frac{\delta U}{\delta M_i} \right) \mathrm{d}\boldsymbol{X}, \tag{2.1}$$

where δ is used to denote the functional derivative and summation over repeated non-particle indices is implied. When U and E depend on χ_i only through its gradient $\frac{\partial \chi_i}{\partial X_j} = F_{ij}$, we can write

$$\{U, E\} = \int \left(\frac{\delta U}{\delta F_{ij}} \frac{\partial}{\partial X_j} \left[\frac{\delta E}{\delta M_i} \right] - \frac{\delta E}{\delta F_{ij}} \frac{\partial}{\partial X_j} \left[\frac{\delta U}{\delta M_i} \right] \right) \mathrm{d}\boldsymbol{X}. \tag{2.2}$$

Now, we substitute functional U in the form

$$U = \int \rho u(\rho, s, \boldsymbol{v}, \mathbb{A}) \mathrm{d}\boldsymbol{x}. \tag{2.3}$$

To find equations, we assume that all fields are compactly supported and so there are no boundary terms (alternatively, periodic boundary condition could be considered). Transforming to the reference frame, we find

$$U = \int \rho_0 u \left(\frac{\rho_0}{J}, \frac{S_0}{\rho_0}, \frac{\boldsymbol{M}}{\rho_0}, \mathbb{F}^{-1} \right) \mathrm{d}\boldsymbol{X}, \tag{2.4}$$

where S_0 is the entropy density in reference frame and $J = \det \mathbb{F}$. Now, we formally evaluate the variation δU when $\mathbb{F}$ and $\boldsymbol{M}$ vary. As a shorthand notation, we will write u_ρ for partial derivative of u with respect to ρ (and similarly for other variables).

$$\begin{aligned} \delta U &= \int \left(-\frac{\rho_0^2}{J^2} u_\rho \delta J + u_{v_i} M_i + \rho_0 u_{A_{kl}} \delta F^{-1}_{kl} \right) \mathrm{d}\boldsymbol{X} \\ &= \int \left(-\frac{\rho_0^2}{J} u_\rho F^{-1}_{ji} \delta F_{ij} + u_{v_i} M_i - \rho_0 u_{A_{kl}} F^{-1}_{ki} F^{-1}_{jl} \delta F_{ij} \right) \mathrm{d}\boldsymbol{X}. \end{aligned} \tag{2.5}$$

From this, we read

$$\begin{aligned} \frac{\delta U}{\delta F_{ij}} &= -\frac{\rho_0^2}{J} u_\rho F^{-1}_{ji} - \rho_0 u_{A_{kl}} F^{-1}_{ki} F^{-1}_{jl}, \\ \frac{\delta U}{\delta M_i} &= u_{vi}. \end{aligned} \tag{2.6}$$

As a next step in the derivation, we substitute (2.6) into (2.2) and use $F^{-1}_{ji} \frac{\partial}{\partial X_j} = \frac{\partial}{\partial x_i}$. This way, we obtain:

$$\begin{aligned} \left\{ \int \rho u \, \mathrm{d}\boldsymbol{x}, \int \rho e \, \mathrm{d}\boldsymbol{x} \right\} = &- \int \left(\rho^2 u_\rho \partial_i e_{v_i} + \rho u_{A_{kl}} A_{ki} \partial_l e_{v_i} \right) \mathrm{d}\boldsymbol{x} \\ &+ \int \left(\rho^2 e_\rho \partial_i u_{v_i} + \rho e_{A_{kl}} A_{ki} \partial_l u_{v_i} \right) \mathrm{d}\boldsymbol{x} \end{aligned} \tag{2.7}$$

The reversible part of SHTC equations follow from (2.7) and from

$$\begin{aligned} \left\{ \int \rho u \, \mathrm{d}\boldsymbol{x}, \int \rho e \, \mathrm{d}\boldsymbol{x} \right\} &= \frac{\mathrm{d}}{\mathrm{d}t} \int \rho u \, \mathrm{d}\boldsymbol{x} \\ &= \int \frac{\mathrm{d}}{\mathrm{d}t} \Big[\rho_0 u(t, \chi(t, \boldsymbol{X})) \Big] \mathrm{d}\boldsymbol{X} \\ &= \int \rho_0 \left[\frac{\partial u}{\partial t} + \frac{\partial u}{\partial x_i} \frac{\partial \chi_i}{\partial t} \right] \mathrm{d}\boldsymbol{X} \\ &= \int \rho \dot{u} \, \mathrm{d}\boldsymbol{x} \\ &= \int \rho (u_\rho \dot{\rho} + u_s \dot{s} + u_{v_i} \dot{v}_i + u_{A_{ij}} \dot{A}_{ij}) \, \mathrm{d}\boldsymbol{x} \end{aligned} \tag{2.8}$$

where $\dot{\varphi} = \partial_t \varphi + v_i \partial_i \varphi$ denotes the material time derivative and e is the specific energy, which satisfies $e_{\boldsymbol{v}} = \boldsymbol{v}$, $e_s = T$ and $e_\rho = \frac{p}{\rho^2}$. Comparing (2.7) and (2.8),

we deduce a partial differential system:

$$\begin{aligned}
\dot{\rho} &= -\rho \operatorname{div} \boldsymbol{v}, \\
\dot{s} &= 0, \\
\dot{\boldsymbol{v}} &= -\frac{\nabla p}{\rho} - \frac{1}{\rho} \operatorname{div} \mathbb{S}, \\
\dot{\mathbb{A}} &= -\mathbb{A} \nabla \boldsymbol{v},
\end{aligned} \tag{2.9}$$

where $\mathbb{S} = \rho \mathbb{A}^T e_{\mathbb{A}}$. The shear stress tensor $\mathbb{S}$ is symmetric, as follows from the assumption of rotational symmetry. Indeed, if e depends on $\mathbb{A}$ only through $\mathbb{G} = \mathbb{A}^T \mathbb{A}$, then $\mathbb{S} = 2\rho \, \mathbb{G} e_{\mathbb{G}}$, which is symmetric because $\mathbb{G}$ and $e_{\mathbb{G}}$ are commutative symmetric matrices.

Finally, a dissipative relaxation term is added into the equation for distortion accompanied by the corresponding entropy production:

$$\begin{aligned}
\dot{\rho} &= -\rho \operatorname{div} \boldsymbol{v}, \\
\dot{s} &= \frac{1}{T\theta} |e_{\mathbb{A}}|_F^2, \\
\dot{\boldsymbol{v}} &= -\frac{\nabla p}{\rho} - \frac{1}{\rho} \operatorname{div} \mathbb{S}, \\
\dot{\mathbb{A}} &= -\mathbb{A} \nabla \boldsymbol{v} - \frac{1}{\theta} e_{\mathbb{A}},
\end{aligned} \tag{2.10}$$

where

$$\theta = \frac{\tau c_s^2}{3} |\det \mathbb{A}|^{-\frac{5}{3}} \tag{2.11}$$

and c_s is shear sound speed. Once relaxation is introduced, $\mathbb{A}$ can no longer be assumed equal to $\nabla \chi$ with the possibility of $\operatorname{curl} \mathbb{A} \neq 0$. The irreversible terms follow from a dissipation potential [31, 36]

$$\Xi = \int \frac{1}{2\tau} A_{ij}^* A_{ij}^* \tag{2.12}$$

(where $*$ indicates conjugate entropic variables). The equations is thus compatible with the GENERIC framework [37, 38].

Compare this to classical equations of non-linear elasticity and Navier-Stokes equations, where material is a fluid as long as internal energy does not depend on $\mathbb{A}$ (other than through $\rho = \rho_0 \det \mathbb{A}$) and the distinction between solid and fluid states is sharp. Navier-Stokes equations can be formally derived from SHTC equations using Chapman-Enskog reduction when c_s approaches infinity [31].

2.2 Response to an impulse of shear

To illustrate the difference between Navier-Stokes system and SHTC equations as a fluid model, let us consider shear flow in $\mathbb{R}^3$, with velocity field

$$\boldsymbol{v} = \begin{pmatrix} v(t, y) \\ 0 \\ 0 \end{pmatrix} \tag{2.13}$$

and constant pressure $p = 0$. Substituting this ansatz into the Navier-Stokes system (it does not matter whether the fluid is deemed compressible or not) provides one nontrivial equation:

$$\partial_t v = \nu \partial_{yy} v. \tag{2.14}$$

When we search for Green function, i.e. solution for initial state described by the Dirac delta

$$v_G(0, y) = \delta_0(y), \tag{2.15}$$

we obtain the Gaussian

$$v_G(t, y) = \frac{1}{\sqrt{4\pi t\nu}} \exp\left(-\frac{y^2}{4t\nu}\right). \tag{2.16}$$

The function has unbounded support for all $t > 0$, which signifies instantaneous response in direction perpendicular to the shear.

Next, let us perform the same procedure but with SHTC equations, expressed in terms of $\mathbb{G} = \mathbb{A}^T\mathbb{A}$:

$$\begin{aligned} \dot{\boldsymbol{v}} &= -\frac{\nabla p}{\rho} + \frac{1}{\rho} \operatorname{div}\left(2\rho\mathbb{G}e_{\mathbb{G}}\right), \\ \dot{\mathbb{G}} &= -\mathbb{G}\nabla\boldsymbol{v} - \nabla\boldsymbol{v}^T\mathbb{G} - \frac{1}{\theta}e_{\mathbb{G}}, \end{aligned} \tag{2.17}$$

where, in addition to (2.13), $s = 0$ and $p = 0$, suppose

$$\mathbb{G} = \begin{pmatrix} 1 & \sigma(t,y) & 0 \\ \sigma(t,y) & 1 & 0 \\ 0 & 0 & 1 \end{pmatrix}. \tag{2.18}$$

Following [39], we relate relaxation time to kinematic viscosity by

$$\tau = \frac{6\nu}{c_s^2} \tag{2.19}$$

and write energy as

$$e = \frac{v^2}{2} + \frac{c_0^2}{2}\left(1 - \frac{\rho}{\rho_0}\right)^2 + \frac{c_s^2}{4}|\operatorname{dev}\mathbb{G}|_F^2 \tag{2.20}$$

where

$$\operatorname{dev}\mathbb{M} = \mathbb{M} - \frac{\operatorname{tr}\mathbb{M}}{d}\mathbb{I} \tag{2.21}$$

denotes the deviatoric part and $|\cdot|_F$ is the Frobenius norm. The matrix derivative is then just

$$e_{\mathbb{G}} = \frac{c_s^2}{2}\operatorname{dev}\mathbb{G} \tag{2.22}$$

Unfortunately, even simple shear is too complex to solve analytically using SHTC model. For this reason, a linearization is needed with respect to $\sigma \ll 1$. Under this assumption, we may write

$$\begin{aligned} \partial_t\boldsymbol{v} &= -c_s^2 \operatorname{div}\operatorname{dev}\mathbb{G}, \\ \partial_t\mathbb{G} &= -\nabla\boldsymbol{v} - \nabla\boldsymbol{v}^T - \frac{c_s^2}{\nu}\operatorname{dev}\mathbb{G}. \end{aligned} \tag{2.23}$$

This system provides two non-trivial scalar equations:

$$\begin{aligned} \partial_t v &= -c_s^2 \partial_y \sigma \\ \partial_t \sigma &= -\partial_y v - \frac{c_s^2}{\nu}\sigma. \end{aligned} \tag{2.24}$$

When we put them together, we find a dissipative wave equation (also called *telegrapher's equation* [40])

$$\frac{\nu}{c_s^2}\partial_{tt} v + \partial_t v = \nu \partial_{yy} v, \tag{2.25}$$

which, compared to (2.14), contains an extra term vanishing for $c_s \to \infty$. The Green function is (see [41] for computational procedure):

$$v_G(y,t) = \frac{1}{2c_s} e^{-tc_s^2/2\nu}\, \delta\left(t - \frac{|y|}{c_s}\right) + \frac{c_s}{4\nu} e^{-tc_s^2/2\nu} \left(I_0(\xi) + \frac{tc_s^2}{2\nu\xi} I_1(\xi)\right) H\left(t - \frac{|y|}{c_s}\right) \tag{2.26}$$

where I_k are modified Bessel functions of first kind, H denotes the Heaviside function and

$$\xi = \frac{c_s^2}{2\nu}\sqrt{t^2 - \frac{y^2}{c_s^2}}. \tag{2.27}$$

The Green function (distribution) (2.26) is composed of exponentially decaying Dirac and a function which is close to the Gaussian but supported inside the strip $\{|y| \leq c_s t\}$. Thus, finite speed of information is guaranteed. Using the asymptotic behavior of modified Bessel functions:

$$I_k(\xi) \sim \frac{e^{\xi}}{\sqrt{2\pi\xi}}, \qquad \xi \to \infty, \tag{2.28}$$

is not difficult to see that (2.26) converges (in distributions) to (2.16) for $c_s \to \infty$ and fixed ν. Hence, general solution $v_0 * v_G$ to initial value problem will converge to Navier-Stokes solution.

2.3 Discrete approximation and balance laws

Following [7], we proceed with the derivation of SPH-like discretization of SHTC model. A conservative particle approximation of the reversible dynamics can be generated from Poisson bracket formula (2.7) by replacing integrals with summation symbols:

$$\begin{aligned} &\sum_a m_a \left(u_{\rho_a}\dot{\rho}_a + u_{s_a}\dot{s}_a + u_{\boldsymbol{v}_a}\cdot\dot{\boldsymbol{v}}_a + u_{\mathbb{A}_a} : \dot{\mathbb{A}}_a\right) \\ &= -\sum_a m_a \left(\rho_a u_\rho \operatorname{div}_a\{e_{\boldsymbol{v}}\} + u_{\mathbb{A}_a} : \mathbb{A}_a \nabla_a\{e_{\boldsymbol{v}}\}\right) \\ &\quad + \sum_a m_a \left(\rho_a e_\rho \operatorname{div}_a\{u_{\boldsymbol{v}}\} + e_{\mathbb{A}_a} : \mathbb{A}_a \nabla_a\{u_{\boldsymbol{v}}\}\right), \end{aligned} \tag{2.29}$$

where div_a and ∇_a are discrete approximations of divergence and gradient, that depend only on functional values at nodal points $\boldsymbol{x}_a$ and which we specify later.

Since u_{ρ_a}, u_{s_a}, u_{v_a}, $u_{\mathbb{A}}$ are arbitrary and $e_{\boldsymbol{v}} = \boldsymbol{v}$, $e_\rho = \frac{p}{\rho^2}$, we deduce

$$\begin{aligned}
\dot{\rho}_a &= -\rho_a \operatorname{div}_a\{e_{\boldsymbol{v}}\}, \\
\dot{s}_a &= 0, \\
\dot{\boldsymbol{v}}_a &= -\frac{1}{\rho_a}\nabla_a^*\{p\} - \nabla_a^*\{\mathbb{S}\}, \\
\dot{\mathbb{A}}_a &= -\mathbb{A}_a \nabla_a\{\boldsymbol{v}\}.
\end{aligned} \tag{2.30}$$

where $\partial_{a,i}^*\{\varphi\}$ denotes a different particle approximation of gradient which is dual to $\partial_{a,i}\{\varphi\}$ in the sense that

$$\sum_a \frac{m_a}{\rho_a}\psi_a \partial_{a,i}^*\{\varphi\} = -\sum_a \frac{m_a}{\rho_a}\partial_{a,i}\{\psi\}\varphi_a. \tag{2.31}$$

Various conservation laws are connected to consistency properties of discrete operator $\partial_{a,i}\{\varphi\}$, as is stated in the following theorem:

Theorem 7. *Let $\rho_a(t)$, $s_a(t)$, $\boldsymbol{v}_a(t)$, $\mathbb{A}_a(t)$, $\boldsymbol{x}(t)$ be C^1 solution of (2.30) and let $\mathbb{S}$ be symmetric. Then*

1. *The total energy $\sum_a m_a e_a$ and entropy $\sum_a m_a s_a$ are conserved.*
2. *If $\partial_{a,i}\{\varphi\} = \partial_i\varphi(\boldsymbol{x}_a)$ for any constant function φ (zero-order consistency), then linear momentum is conserved.*
3. *If $\partial_{a,i}\{\varphi\} = \partial_i\varphi(\boldsymbol{x}_a)$ for any linear function φ (first-order consistency), then angular momentum is conserved.*

Proof. Entropy conservation is trivial and energy conservation immediately follows from formulation (2.29), when we substitute $u = e$. To obtain conservation of z-component of linear momentum, we set $u = \sum_a m_a \boldsymbol{v}_a \cdot \hat{\boldsymbol{z}}$. Then

$$u_{\boldsymbol{v}_a} = \hat{\boldsymbol{z}} \tag{2.32}$$

and u_{ρ_a}, u_{s_a}, $u_{\mathbb{A}}$ are zero. Assuming the discrete derivative is at least zero-order consistent, the left-hand side in (2.29) vanishes. To obtain conservation of z-component of angular momentum, we substitute

$$u_{\boldsymbol{v}_a} = x\hat{\boldsymbol{y}} - y\hat{\boldsymbol{x}} \tag{2.33}$$

in (2.29). (This cannot be realized as a partial derivative of a function $u = u(\rho, s, \boldsymbol{v}, \mathbb{A})$. However, validity of (2.29) can be easily extended to such cases by summation of (2.30).) Eventually, we obtain

$$\begin{aligned}
&\frac{\mathrm{d}}{\mathrm{d}t}\sum_a m_a u_{\boldsymbol{v}_a}\cdot\boldsymbol{v}_a = \sum_a m_a u_{\boldsymbol{v}_a}\cdot\dot{\boldsymbol{v}}_a = \\
&= -\sum_a m_a\left(-\rho_a e_\rho \operatorname{div}_a\{u_{\boldsymbol{v}}\} + \frac{1}{\rho}\mathbb{S} : \nabla_a\{u_{\boldsymbol{v}}\}\right) = 0,
\end{aligned} \tag{2.34}$$

assuming first-order consistency (as $\operatorname{div} u_{\boldsymbol{v}} = 0$ and $\nabla u_{\boldsymbol{v}}$ is anti-symmetric). Proofs for x-components and y-components of linear and angular momentum are completely analogical. □

Inclusion of relaxation in the discrete formulation is straightforward because the irreversible terms do not involve any derivatives.

$$\begin{aligned}
\dot{\rho}_a &= -\rho_a \operatorname{div}_a\{e_{\boldsymbol{v}}\},\\
\dot{s}_a &= \frac{1}{T_a\theta_a}|e_{\mathbb{A}_a}|^2,\\
\dot{\boldsymbol{v}}_a &= -\frac{1}{\rho_a}\nabla_a^*\{p\} - \nabla_a^*\left\{\mathbb{S}\right\},\\
\dot{\mathbb{A}}_a &= -\mathbb{A}_a\nabla_a\{\boldsymbol{v}\} - \frac{1}{\theta_a}e_{\mathbb{A}_a}.
\end{aligned} \tag{2.35}$$

It is clear that this will not violate any discrete conservation law, with the only exception that entropic equality becomes an entropic inequality.

2.4 Renormalized operators

In previous section, we studied the discrete conservation laws of SHTC equations. We found that we can expect conservation of angular momentum provided that discrete approximation of derivative is exact for polynomials of first degree. This is, unfortunately, not satisfied by the operator introduced in section 1.2:

$$\partial^0_{a,i}\{\varphi\} = -\frac{1}{\rho_a}\sum_b m_b\varphi_{ab}\partial_i W_{h,ab}, \quad \forall\varphi, \tag{2.36}$$

which is exact only for constants. Therefore, a stronger caliber is needed, and this is the *renormalized operator*. Several variants of renormalized SPH operators can be found in literature [12]. In this work, we use the following one:

$$\partial^1_{a,i}\{\varphi\} = -\frac{1}{\rho_a}\sum_b m_b\varphi_{ab}R^{-1}_{a,ji}\partial_j W_{h,ab}, \quad \forall\varphi, \tag{2.37}$$

or, equivalently, in vectorial notation

$$\nabla^1_a\{\varphi\} = -\frac{1}{\rho_a}\sum_b m_b\varphi_{ab}R^{-T}\nabla W_{h,ab}, \quad \forall\varphi, \tag{2.38}$$

where the renormalization matrix R is provided by equation

$$R_a = -\frac{1}{\rho_a}\sum_b m_b\boldsymbol{x}_{ab}\otimes\nabla W_{h,ab}. \tag{2.39}$$

It is clear that such operator is first-order consistent because

$$\nabla^1_a\{\boldsymbol{x}\} = \left(\sum_b m_b\boldsymbol{x}_{ab}\otimes\nabla W_{h,ab}\right)\left(\sum_b m_b\boldsymbol{x}_{ab}\otimes\nabla W_{h,ab}\right)^{-1} = \mathbb{I}. \tag{2.40}$$

Moreover, it has a natural interpretation as a weighted least square solution to an over-determined linear system $\nabla_a\{\varphi\}\cdot\boldsymbol{x}_{ab}\approx\varphi_{ab}$, for all particle labels a, b (see [42]). We formulate this in the next theorem.

Theorem 8. *For fixed a, suppose that R_a is invertible and $r_{ab} > 0$ for all b. Then $\nabla_a^1\{\varphi\}$ is the unique minimizer of*

$$\sum_b \omega_{ab} |\nabla_a^1\{\varphi\} \cdot \boldsymbol{x}_{ab} - \varphi_{ab}|^2 \tag{2.41}$$

where weights ω_{ab} are given by:

$$\omega_{ab} = -m_b \frac{W'_{h,ab}}{r_{ab}}. \tag{2.42}$$

Proof. Note that (due to non-increasing property of kernel) $\omega_{ab} \geq 0$ for every pair a, b. We search for stationary point of a functional

$$\mathcal{F}(\boldsymbol{\xi}) = \frac{1}{2} \sum_b \omega_{ab} |\boldsymbol{\xi} \cdot \boldsymbol{x}_{ab} - \varphi_{ab}|^2. \tag{2.43}$$

This way, we obtain

$$0 = \mathrm{d}\mathcal{F} = -\sum_b \omega_{ab} (\boldsymbol{\xi} \cdot \boldsymbol{x}_{ab} - \varphi_{ab})(\mathrm{d}\boldsymbol{\xi} \cdot \boldsymbol{x}_{ab}) \tag{2.44}$$

for every $\mathrm{d}\boldsymbol{\xi}$. Hence

$$\begin{aligned}
0 &= -\sum_b \omega_{ab} (\boldsymbol{\xi} \cdot \boldsymbol{x}_{ab} - \varphi_{ab}) \boldsymbol{x}_{ab}, \\
0 &= -\frac{1}{\rho_a} \sum_b m_b (\boldsymbol{\xi} \cdot \boldsymbol{x}_{ab} - \varphi_{ab}) \nabla W_{h,ab}, \\
0 &= R_a^T \boldsymbol{\xi} + \frac{1}{\rho_a} \sum_b m_b \varphi_{ab} \boldsymbol{x}_{ab} \nabla W_{h,ab}. \\
\boldsymbol{\xi} &= -\frac{1}{\rho_a} \sum_b m_b \varphi_{ab} R_a^{-T} \nabla W_{h,ab}.
\end{aligned} \tag{2.45}$$

Hence, there is only one stationary point $\boldsymbol{\xi} = \nabla_a^1\{\varphi\}$. It is easy to see that $\mathcal{F}$ is coercive and ξ must therefore be an argument of minimum. □

Regarding the invertibility of R_a, it is easy to see that the matrix is symmetric positive semi-definite. To make it invertible, it is enough that for every vector $\boldsymbol{c}$, there is b such that $\boldsymbol{c} \cdot \boldsymbol{x}_{ab} \neq 0$ and $W'_{h,ab} \neq 0$. That is to say, particle a and particles in its vicinity (defined by the support of the kernel) must not be co-planar. When it comes to performance, the inversion of the matrix is not too problematic because it is just a $d \times d$ matrix for every particle, so inverting all of them has $O(N)$ complexity, where N is particle number.

Finally, it is an easy algebraic exercise to show that the dual differential operator $\partial_{a,i}^*$ satisfying (2.31) is of the form:

$$\partial_{a,i}^* \{\psi\} = \rho_a \sum_b m_b \left(\frac{\psi_a R_{a,ji}^{-1}}{\rho_a^2} + \frac{\psi_b R_{b,ji}^{-1}}{\rho_b^2} \right) \partial_j W_{h,ab}. \tag{2.46}$$

2.5 Time discretization

We now look at a time discretization of particle approximation in SHTC model. Unfortunately, we can no longer use symplectic integration because of the variable $\mathbb{A}$. There are many discretizations that could be implemented, but we prefer to keep it backward compatible with the classical SPH scheme, which is known to work sufficiently well. For this reason, we use a mixture of first and zero-order SPH derivatives:

$$\begin{aligned}
\dot{\rho}_a &= -\rho_a \operatorname{div}_a^0\{e_{\boldsymbol{v}}\},\\
\dot{s}_a &= \frac{1}{T_a\theta_a}|e_{\mathbb{A}_a}|^2,\\
\dot{\boldsymbol{v}}_a &= -\frac{1}{\rho_a}\nabla_a^{0*}\{p\} + \nabla_a^{1*}\{\mathbb{S}\},\\
\dot{\mathbb{A}}_a &= -\mathbb{A}_a\nabla_a^1\{\boldsymbol{v}\} - \frac{1}{\theta_a}e_{\mathbb{A}_a}.
\end{aligned} \tag{2.47}$$

The z-component of angular momentum will be still conserved because in (2.34)

$$\operatorname{div}_a^0\{u_{\boldsymbol{v}}\} = 0 \tag{2.48}$$

for $u_{\boldsymbol{v}}$ is orthogonal to $\boldsymbol{x}$. The density then does not need to be evolved and (1.14) can be used instead and for energy which is only a function of ρ and $\boldsymbol{v}$, the classical SPH is recovered. (As a third option how to compute density, we could use $\rho = \frac{\rho_0}{\det\mathbb{A}}$, where ρ_0 is referential density, but our numerical experiments revealed that this is less stable.) We also like to keep reversibility in the special case $\tau = \infty$. Hence, we use a modification of Verlet integrator with relaxation step implemented using Runge-Kutta (RK4) subiterations.

$$\begin{aligned}
\boldsymbol{v}_a\left(t_{k+\frac{1}{2}}\right) &= \boldsymbol{v}_a(t_k) + \frac{\delta t}{2m_a}\boldsymbol{f}_a(t_k),\\
\boldsymbol{x}_a\left(t_{k+\frac{1}{2}}\right) &= \boldsymbol{x}_a(t_k) + \frac{\delta t}{2}\boldsymbol{v}_a\left(t_{k+\frac{1}{2}}\right),\\
s_a(t_{k+1}) &= s_a(t_k) + \delta t\zeta_a(t_k),\\
\tilde{\mathbb{A}}_a(t_k) &= \mathbb{A}_a(t_k)\left(\mathbb{I} - \frac{\delta t}{2}\mathbb{L}_a\left(t_{k+\frac{1}{2}}\right)\right)\left(\mathbb{I} + \frac{\delta t}{2}\mathbb{L}_a\left(t_{k+\frac{1}{2}}\right)\right)^{-1},\\
\mathbb{A}_a(t_{k+1}) &= \tilde{\mathbb{A}}(t_k) + \frac{\delta t}{6}\Big(\mathbb{K}_{1,a}(t_k) + 2\mathbb{K}_{2,a}(t_k) + 2\mathbb{K}_{3,a}(t_k) + \mathbb{K}_{4,a}(t_k)\Big)\\
\boldsymbol{x}_a(t_{k+1}) &= \boldsymbol{x}_a\left(t_{k+\frac{1}{2}}\right) + \frac{\delta t}{2}\boldsymbol{v}_a\left(t_{k+\frac{1}{2}}\right),\\
\boldsymbol{v}_a(t_{k+1}) &= \boldsymbol{v}_a\left(t_{k+\frac{1}{2}}\right) + \frac{\delta t}{2m_a}\boldsymbol{f}_a(t_{k+1}),
\end{aligned} \tag{2.49}$$

where

$$\begin{aligned}
\boldsymbol{f}_a &= -m_a\frac{1}{\rho_a}\nabla_a^{0*}\{p\} + m_a\nabla_a^{1*}\{\mathbb{S}\},\\
\zeta_a &= \frac{1}{T_a\theta_a}|e_{\mathbb{A}_a}|^2,\\
\mathbb{L}_a &= \nabla_a^1\{\boldsymbol{v}\},\\
\mathbb{K}_{i,a}(t_k) &= -\frac{1}{\theta_a}\epsilon_{\mathbb{A}_a}\Big|_{\mathbb{A}_a=\tilde{\mathbb{A}}_a(t_k)+b_i\,\delta t\,\mathbb{K}_{i-1,a}(t_k)},
\end{aligned} \tag{2.50}$$

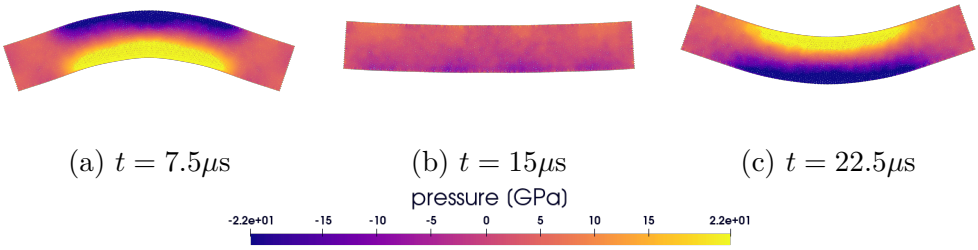

(a) $t = 7.5\mu$s (b) $t = 15\mu$s (c) $t = 22.5\mu$s

Figure 2.1: Plate in three different time-steps. Color indicates pressure. Simulation of 10000 particles.

constant	A	ω	α	a_1	a_2	L	W
value	4.3369E-5	2.3597E+5	78.834	56.6368	57.6455	6	1
unit	m	s^{-1}	1	1	1	cm	cm

Table 2.1: Parameters used in beryllium plate benchmark for defining geometry and initial condition.

and $(b_1, b_2, b_3, b_4) = (1, \frac{1}{2}, \frac{1}{2}, 1)$.

2.6 Bending of beryllium plate

In this two-dimensional example, we study an elastic solid ($\tau = \infty$), with specific energy given by (2.20) The physical values are $\rho = 1850\text{kg/m}^3, c_0 = c_s = 9046.59\text{m/s}$. The initial shape of the solid is

$$\Omega_0 = \left(-\frac{L}{2}, \frac{L}{2}\right) \times \left(-\frac{W}{2}, \frac{W}{2}\right). \tag{2.51}$$

We prescribe initial condition $\rho(0) = \rho_0$, $\mathbb{A}(0) = \mathbb{I}$ and

$$\boldsymbol{v}(t = 0, \xi) = A\,\omega \begin{pmatrix} 0 \\ a_1 \left(\sinh \xi + \sin \xi\right) - a_2 \left(\cosh \xi + \cos \xi\right), \end{pmatrix} \tag{2.52}$$

where $\xi = \alpha \left(x + \frac{L}{2}\right)$. Values of relevant constants are shown in Table 2.1. In this example, the plate was subject to *tensile instability*, which is a known numerical artifact in SPH [2] and which occurs in regions of negative pressure. The tensile instability causes breaking of the plate. We resolved this problem by adding a small *tensile penalty* to the energy. The details can be found in paper [7]. Figure 2.1 shows the evolution of the plate and Figure 2.2 the balance of different energy contributions in time. The simulation is compared to a referential solution in Figure 2.3 by measuring the height of the central material point.

2.7 Lid-driven cavity

The same equations and energy (2.20) can be used to model viscous flow when τ is finite. We demonstrate this in a classical lid-driven cavity benchmark. In this

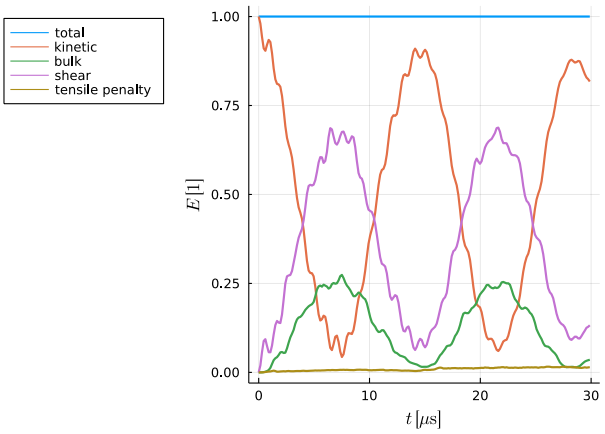

Figure 2.2: Four contributions to energy (2.20) plotted against time. The relative energy error was within 10^{-5}.

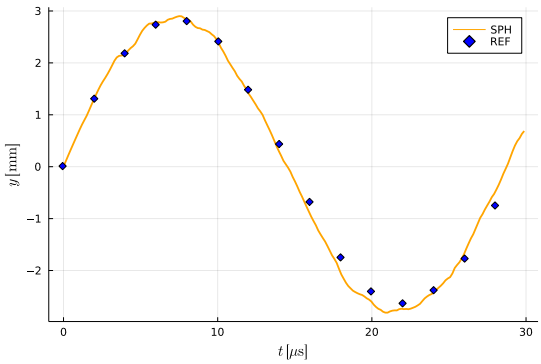

Figure 2.3: Height of the central material point against time. Orange line is SPH result and blue markers shows a referential solution computed using finite volume method [43].

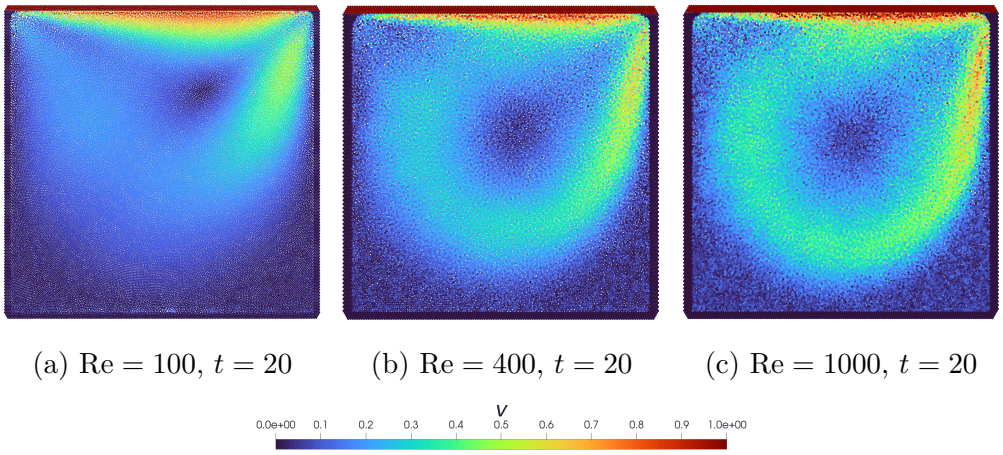

(a) Re = 100, $t = 20$ (b) Re = 400, $t = 20$ (c) Re = 1000, $t = 20$

Figure 2.4: Velocity field in the Newtonian lid-driven cavity benchmark.

dimensionless problem, we model Newtonian incompressible flow inside a square $\Omega = (0, 1) \times (0, 1)$ with no-slip boundary condition on left, bottom and right walls and prescribed velocity

$$\boldsymbol{v}_{\text{lid}} = \begin{pmatrix} 1 \\ 0 \end{pmatrix} \tag{2.53}$$

at the top. Unfortunately, in our SPH-SHTC model, we cannot substitute $c_s = c_0 = \infty$, but to get a reasonable approximation, it is enough to set $c_s = c_0 = 20$ (so that shear and longitudinal waves spreads 20 times faster than maximum fluid velocity). Viscosity is given by

$$\nu = \frac{L_{\text{char}} U_{\text{char}}}{\text{Re}}, \tag{2.54}$$

where $L_{\text{char}} = 1$, $U_{\text{char}} = 1$ and the Reynolds number Re has various values. The walls were implemented using dummy particles. Flux through horizontal and vertical centerline was measured and compared to reference solution [44] with reasonable agreement (Figure 2.6). An interesting feature of this simulation is that whereas velocity field is visibly converging to stationary state (Figure 2.4), the distortion forms a non-stationary spiral pattern of shear waves (Figure 2.5).

2.8 Summary

In conclusion, we obtained a conservative particle approximation of SHTC equations for fluids and solids. The numerical scheme was tested in benchmarks. A good agreement with reference was obtained in both solid and fluid regime. (For more benchmarks, we refer to [7].) In future, our work can be extended to model multiphase flows. The ease of describing phase change in SHTC model provides potential applications in additive manufacturing.

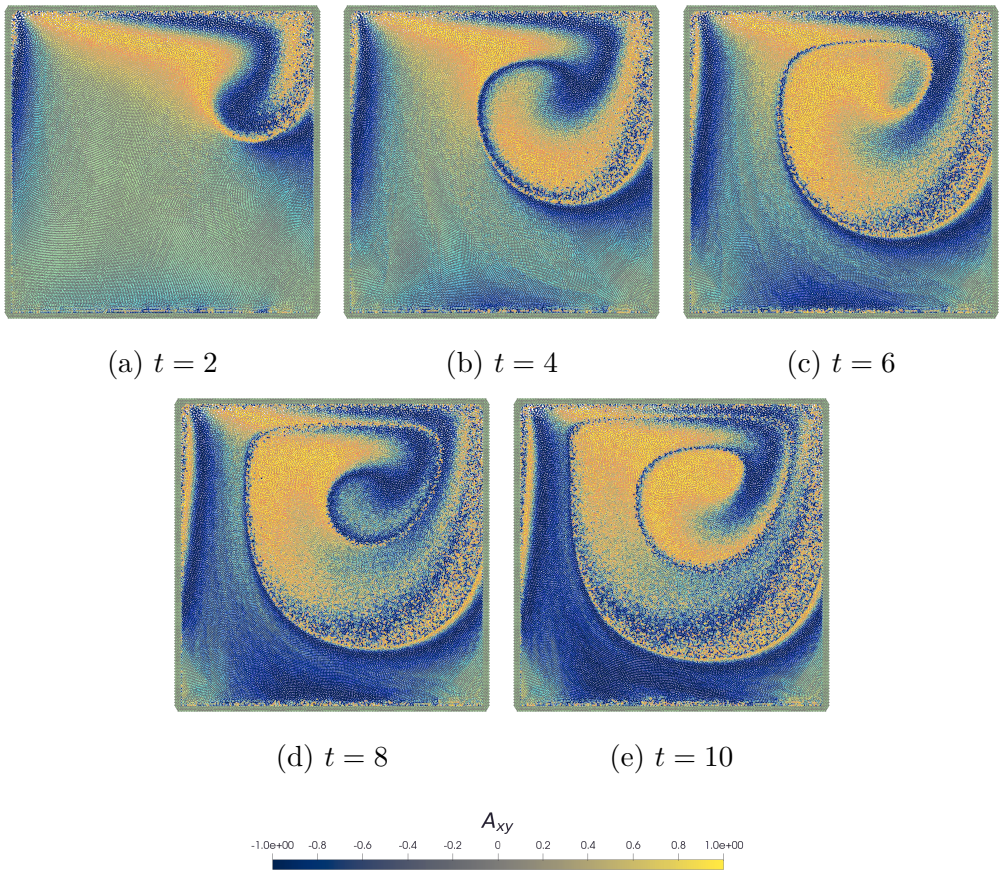

(a) $t = 2$ (b) $t = 4$ (c) $t = 6$

(d) $t = 8$ (e) $t = 10$

Figure 2.5: Evolution of the distortion field in Newtonian lid-driven cavity benchmark for $\mathrm{Re} = 100$.

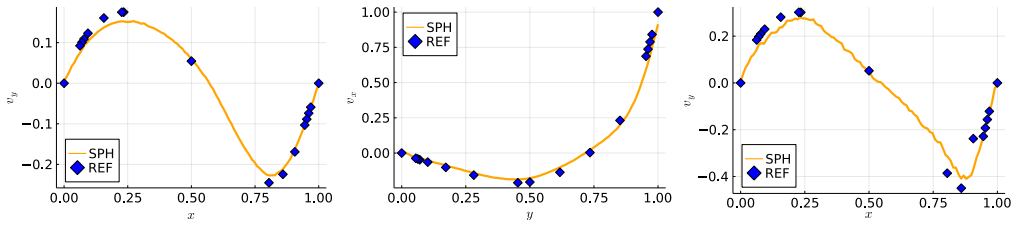

(a) v_y along x-centerline, $\mathrm{Re} = 100$, $t = 10$ (b) v_x along y-centerline, $\mathrm{Re} = 100$, $t = 10$ (c) v_y along x-centerline, $\mathrm{Re} = 400$, $t = 20$

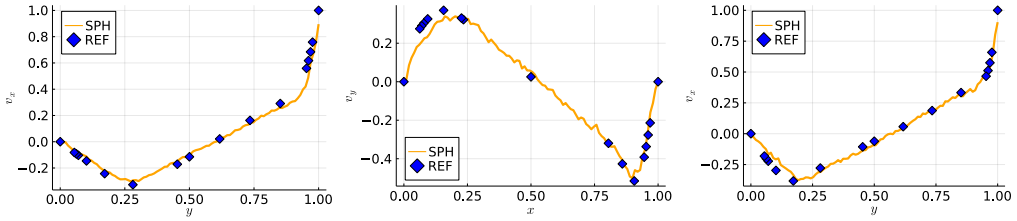

(d) v_x along y-centerline, $\mathrm{Re} = 400$, $t = 20$ (e) v_y along x-centerline, $\mathrm{Re} = 1000$, $t = 20$ (f) v_x along y-centerline, $\mathrm{Re} = 1000$, $t = 20$

Figure 2.6: Plot of transverse velocities along lines $x = \frac{1}{2}$ and $y = \frac{1}{2}$ in the Newtonian lid-driven cavity benchmark. Decent agreement with reference is achieved. With growing Reynolds numbers, however, distortion $\mathbb{A}$ has increasingly complicated dynamics, which makes it difficult to resolve viscous stress accurately. Therefore, we see some oscillations in the curves for $\mathrm{Re} = 1000$.

3. SPH for superfluid helium-4

Helium-4 is liquid below 4.5 K at saturated vapor pressure and, unlike other elements or compounds, does not solidify even when the temperature approaches absolute zero [45]. In 1938 Kapitsa and Allen & Misener independently discovered that the ^{4}He undertakes a second-order transition below the lambda point $T_\lambda = 2.17$K and becomes a *superfluid*. This state of matter is characterized by an unusually long thermal de-Broglie wavelength [46]

$$\lambda = \frac{h}{\sqrt{2\pi m k_B T}},$$

where h is the Planck constant, m is particle mass and k_B is the Boltzmann constant. As the wavelength exceeds mean interparticle distances, the material becomes influenced by Bose-Einstein statistics. Consequently, superfluid helium displays properties that are macro-scale manifestations of quantum physics. Analogically to superconductors, which conduct electricity without resistance, superfluid helium can flow through porous materials and narrow capillaries without friction. When contained in a cup, it leaks by crawling up and over the walls (*Rollin film effect*). A submerged heat source generates waves called *second sound*, contrary to the usual dissipative behavior described by Fourier's law. Superfluid helium has excellent heat conductivity, which makes it irreplaceable in specific high-performance cooling devices [47]. Superfluid responds strongly to even subtle temperature gradients and may convert heat energy to fluid motion (*mechanocaloric effect*). A notorious demonstration is a *superfluid fountain*, where a small heater (resistor or laser) can produce sufficiently strong force to drive superfluid helium against gravity [48, 49].

As theoretically predicted by Lars Onsager in 1949, circulation in superfluid is quantized. His hypothesis was confirmed experimentally by Joe Vinen in 1961. Quantum vortices can form structures, such as lattices and vortex rings. Complicated vortex tangles often lead to chaotic dynamics called *quantum turbulence* [50, 51, 52].

Superfluidity in ^{3}He was discovered in the 1970s by Lee, Osheroff, and Richardson. The substantial difference between the two isotopes is that ^{3}He is a fermion, unlike ^{4}He, which is a boson. To become superfluid, atoms of ^{3}He must form Cooper pairs, which collectively behave as bosons. The pairing is energetically favorable only at ultra-low temperatures $T \sim 3$mK. The theory surrounding ^{3}He is more complicated since it has two superfluid phases, A and B, and interacts strongly with the magnetic field. In this thesis, we focus solely on ^{4}He for simplicity.

3.1 Two-fluid model

A macroscopic mathematical model for superfluid was developed by Tizsa (1938) and theoretically justified by Landau (1941). To describe helium, it uses two velocity fields. This is necessary, since even below the lambda point, helium retains some classical properties. Landau explained this by presence of quantum excitations: *phonons* and *rotons*. These quasi-particles are advected by the *normalflow*

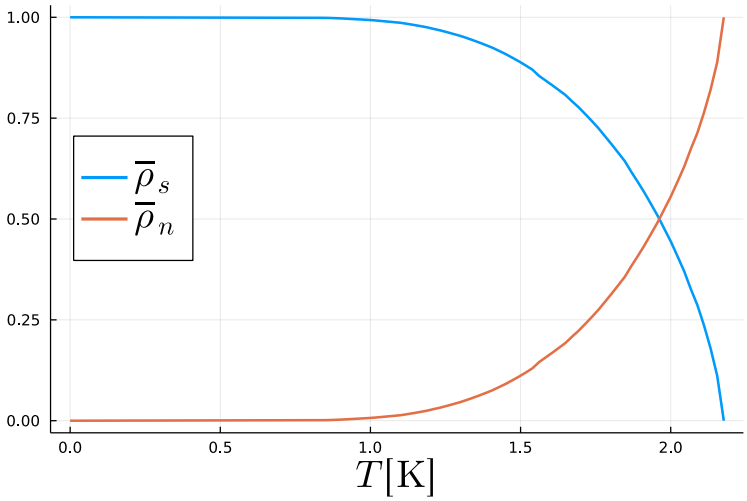

Figure 3.1: Graph of $\overline{\rho}_n$, $\overline{\rho}_s$ against temperature (in Kelvins). Graph created using measured values [53].

velocity $\boldsymbol{v}_n$. Meanwhile, the inviscid flow of condensed helium is associated with the *superflow* velocity $\boldsymbol{v}_s$. Both vectors contribute to the momentum

$$\rho \boldsymbol{v} = \boldsymbol{p} = \rho_n \boldsymbol{v}_n + \rho_s \boldsymbol{v}_s. \tag{3.1}$$

The numbers ρ_n and ρ_s are called normal and super components of density respectively. It would be misleading to think of superfluid as a mixture consisting of atoms of two types [54]. Nonetheless, ρ_n and ρ_s are useful parameters in two-fluid model, which describe the amount of fully condensed helium and the prevalence of quantum properties. We also define relative values

$$\overline{\rho}_n = \frac{\rho_n}{\rho}, \qquad \overline{\rho}_s = \frac{\rho_s}{\rho}, \tag{3.2}$$

which satisfy $\overline{\rho}_n + \overline{\rho}_s = 1$. Note that even when the superfluid has zero momentum, there still can be non-vanishing *counterflow velocity*

$$\boldsymbol{v}_{ns} = \boldsymbol{v}_n - \boldsymbol{v}_s \tag{3.3}$$

The normal relative density depends on temperature T (see Figure 3.1). On the other hand, the total density has approximately constant value $\rho \doteq 125\text{kg/m}^3$.

As shown in [55], the two-fluid model admits a Hamiltonian formulation. The starting point is a quasi-classical bracket for continuum, which in the Lagrangian frame reads

$$\{U, E\} = \int \left(\frac{\delta U}{\delta \chi_i} \frac{\delta E}{\delta M_i} - \frac{\delta E}{\delta \chi_i} \frac{\delta U}{\delta M_i} \right) \mathrm{d}\boldsymbol{X} + \int \left(\frac{\delta U}{\delta \rho_0} \frac{\delta E}{\delta \phi} - \frac{\delta E}{\delta \rho_0} \frac{\delta U}{\delta \phi} \right) \mathrm{d}\boldsymbol{X}, \tag{3.4}$$

where ϕ is the phase of the condensate wave function. As usual, we make the basic assumption that U and E depend on χ and ϕ only through their gradients $F_{ij} = \frac{\partial \chi_i}{\partial X_j}$ and $W_i = \frac{\partial \phi}{\partial X_i}$. This leads to an expression

$$\begin{aligned} \{U, E\} = &\int \left(\frac{\delta U}{\delta F_{ij}} \frac{\partial}{\partial X_j} \left(\frac{\delta E}{\delta M_i} \right) - \frac{\delta E}{\delta F_{ij}} \frac{\partial}{\partial X_j} \left(\frac{\delta U}{\delta M_i} \right) \right) \mathrm{d}\boldsymbol{X} \\ &+ \int \left(\frac{\delta E}{\delta W_i} \frac{\partial}{\partial X_i} \left(\frac{\delta U}{\delta \rho_0} \right) - \frac{\delta U}{\delta W_i} \frac{\partial}{\partial X_i} \left(\frac{\delta E}{\delta \rho_0} \right) \right) \mathrm{d}\boldsymbol{X}. \end{aligned} \tag{3.5}$$

Next, we perform Lagrange to Euler mapping by substituting a function in the form

$$U = \int \rho\, u(\rho, s, \boldsymbol{v}, \boldsymbol{v}_s)\, \mathrm{d}\boldsymbol{x}\,, \tag{3.6}$$

where superfluid velocity is identified with $\nabla\phi$. We then find

$$U = \int \rho_0\, u\left(\frac{\rho_0}{J}, \frac{S_0}{\rho_0}, \frac{\boldsymbol{M}}{\rho_0}, \mathbb{F}^{-T}\boldsymbol{W}\right) \mathrm{d}\boldsymbol{X} \tag{3.7}$$

(where $J = \det \mathbb{F}$) and, therefore, we obtain

$$\begin{aligned}
\frac{\delta U}{\delta F_{ij}} &= -\rho_0 \left(\rho u_\rho F^{-1}_{ji} + u_{v_{s,k}} v_{s,i} F^{-1}_{jk}\right) \\
\frac{\delta U}{\delta M_i} &= u_{v_i} \\
\frac{\delta U}{\delta W_i} &= \rho_0 F^{-1}_{ij} u_{v_{s,j}} \\
\frac{\delta U}{\delta \rho_0} &= u + \rho u_\rho - s u_s - u_{v_i} v_i.
\end{aligned} \tag{3.8}$$

Analogical conclusion can be made about a functional E in the form

$$E = \int \rho e(\rho, s, \boldsymbol{v}, \boldsymbol{v}_s)\, \mathrm{d}\boldsymbol{x}\,. \tag{3.9}$$

We substitute this into (3.5), using $F^{-1}_{jk}\frac{\partial}{\partial X_j} = \frac{\partial}{\partial x_k}$ and

$$\mathrm{d}\left(\frac{\delta U}{\delta \rho_0}\right) = \frac{1}{\rho}\mathrm{d}\left(\rho^2 u_\rho\right) - s\,\mathrm{d}u_s - v_i\,\mathrm{d}u_{v_i} + u_{v_{s,i}}\,\mathrm{d}v_{s,i}\,. \tag{3.10}$$

At the end of the day, we find

$$\begin{aligned}
\left\{\int \rho u\,\mathrm{d}\boldsymbol{x}\,, \int \rho e\,\mathrm{d}\boldsymbol{x}\right\} &= \int \rho^2 \left[e_\rho \operatorname{div}(u_{\boldsymbol{v}} + u_{\boldsymbol{v}_s}) - u_\rho \operatorname{div}(e_{\boldsymbol{v}} + e_{\boldsymbol{v}_s})\right] \\
&\quad - \int \rho(\boldsymbol{v} - \boldsymbol{v}_s) \cdot \left[\nabla u_{\boldsymbol{v}}\, e_{\boldsymbol{v}_s} - \nabla e_{\boldsymbol{v}}\, u_{\boldsymbol{v}_s}\right] \\
&\quad - \int \rho s \left(\nabla u_s \cdot e_{\boldsymbol{v}_s} - \nabla e_s \cdot u_{\boldsymbol{v}_s}\right).
\end{aligned} \tag{3.11}$$

Superfluid equations can be inferred from (3.4) by comparing it to

$$\begin{aligned}
\left\{\int \rho u\,\mathrm{d}\boldsymbol{x}\,, \int \rho e\,\mathrm{d}\boldsymbol{x}\right\} &= \frac{\mathrm{d}}{\mathrm{d}t}\left(\int \rho u\,\mathrm{d}\boldsymbol{x}\right) \\
&= \int \rho \left(u_\rho \dot{\rho} + u_s \dot{s} + u_{\boldsymbol{v}} \cdot \dot{\boldsymbol{v}} + u_{\boldsymbol{v}_s} \cdot \dot{\boldsymbol{v}}_s\right),
\end{aligned} \tag{3.12}$$

when e is the specific energy and by performing a localization argument. This yields a system of partial differential equations:

$$\begin{aligned}
\dot{\rho} &= -\rho \operatorname{div}(e_{\boldsymbol{v}} + e_{\boldsymbol{v}_s}) \\
\dot{s} &= \frac{1}{\rho} \operatorname{div}(\rho s e_{\boldsymbol{v}_s}) \\
\dot{\boldsymbol{v}} &= \frac{1}{\rho} \operatorname{div}(\rho(\boldsymbol{v} - \boldsymbol{v}_s) \otimes e_{\boldsymbol{v}_s}) - \frac{1}{\rho}\nabla(\rho^2 e_\rho) \\
\dot{\boldsymbol{v}}_s &= \nabla e^T_{\boldsymbol{v}}(\boldsymbol{v} - \boldsymbol{v}_s) - \frac{1}{\rho}\nabla(\rho^2 e_\rho) + s\nabla e_s.
\end{aligned} \tag{3.13}$$

Finally, the derivatives of energy can be identified from a total differential [56, 57],

$$\mathrm{d}e = \boldsymbol{v}_n \cdot \mathrm{d}\boldsymbol{v} - \overline{\rho}_s \boldsymbol{v}_{ns} \cdot \mathrm{d}\boldsymbol{v}_s + T\mathrm{d}s + \frac{p}{\rho^2}\mathrm{d}\rho. \tag{3.14}$$

Hence, we find

$$\begin{aligned}
\dot{\rho} &= -\rho \operatorname{div} \boldsymbol{v} \\
\dot{s} &= -\frac{1}{\rho} \operatorname{div}(\rho\, \overline{\rho}_s s \boldsymbol{v}_{ns}) \\
\dot{\boldsymbol{v}} &= -\frac{1}{\rho} \operatorname{div}(\rho\, \overline{\rho}_s \overline{\rho}_n \boldsymbol{v}_{ns} \otimes \boldsymbol{v}_{ns}) - \frac{\nabla p}{\rho} \\
\dot{\boldsymbol{v}}_s &= \overline{\rho}_n \nabla \boldsymbol{v}_n^T \boldsymbol{v}_{ns} - \frac{\nabla p}{\rho} + s\nabla T,
\end{aligned} \tag{3.15}$$

which is the reversible part of two-fluid model. It is a closed system of 8 equations for 8 unknowns, provided that the specific energy e is known.

3.2 Comparison to other two-fluid formulations

The system (3.15) can be rewritten by expanding the definition of material derivative as follows:

$$\begin{aligned}
\frac{\partial \rho}{\partial t} &= -\operatorname{div}(\rho \boldsymbol{v}), \\
\frac{\partial (\rho s)}{\partial t} &= -\operatorname{div}(\rho s \boldsymbol{v}_n), \\
\frac{\partial (\rho \boldsymbol{v})}{\partial t} &= -\operatorname{div}(\rho_n \boldsymbol{v}_n \otimes \boldsymbol{v}_n + \rho_s \boldsymbol{v}_s \otimes \boldsymbol{v}_s) - \nabla p, \\
\frac{\partial \boldsymbol{v}_s}{\partial t} &= -\nabla \left(\frac{v_s^2}{2} + \mu \right) + (\nabla \boldsymbol{v}_s^T - \nabla \boldsymbol{v}_s)\boldsymbol{v},
\end{aligned} \tag{3.16}$$

where μ is called *chemical potential* and satisfies

$$\mathrm{d}\mu = -s\mathrm{d}T + \frac{1}{\rho}\mathrm{d}p - \overline{\rho}_n \boldsymbol{v}_{ns} \cdot \mathrm{d}\boldsymbol{v}_{ns}. \tag{3.17}$$

This is identical to the formulation by Landau [58]:

$$\begin{aligned}
\frac{\partial \rho}{\partial t} &= -\operatorname{div}(\rho \boldsymbol{v}), \\
\frac{\partial (\rho s)}{\partial t} &= -\operatorname{div}(\rho s \boldsymbol{v}_n), \\
\frac{\partial (\rho \boldsymbol{v})}{\partial t} &= -\operatorname{div}(\rho_n \boldsymbol{v}_n \otimes \boldsymbol{v}_n + \rho_s \boldsymbol{v}_s \otimes \boldsymbol{v}_s) - \nabla p, \\
\frac{\partial \boldsymbol{v}_s}{\partial t} &= -\nabla \left(\frac{v_s^2}{2} + \mu \right)
\end{aligned} \tag{3.18}$$

up to the extra term $(\nabla \boldsymbol{v}_s^T - \nabla \boldsymbol{v}_s)\boldsymbol{v}$ that vanishes under the constraint $\boldsymbol{\nabla} \times \boldsymbol{v}_s = 0$ (which follows from definition $\boldsymbol{v}_s = \nabla\phi$). However, this is no longer true in HVBK models, where quantum vortex lines are considered infinitesimal and $\boldsymbol{\nabla} \times \boldsymbol{v}_s$ is

generally nonzero (especially when the vortices are polarized). For this reason, (3.16) should be used over (3.18) as a basis for HVBK equations, if one wishes to preserve the Hamiltonian structure. We refer to [55] for more detailed coverage of these nuances. In addition, the formulation (3.15) or (3.16) is more convenient from the numerical point of view. Energy conservation in a numerical scheme derived from (3.18) hinges on the constraint $\boldsymbol{\nabla} \times \boldsymbol{v}_s = 0$, which is difficult to guarantee numerically.

Lastly, let us talk about the impracticality of describing superfluid helium as a mixture of normal and super component. The issue stems from the fact that the equation of continuity

$$\frac{\partial \rho}{\partial t} + \operatorname{div}(\rho \boldsymbol{v}) = 0 \tag{3.19}$$

cannot be split as

$$\begin{aligned} \frac{\partial \rho_n}{\partial t} + \operatorname{div}(\rho_n \boldsymbol{v}_n) &= 0, \\ \frac{\partial \rho_s}{\partial t} + \operatorname{div}(\rho_s \boldsymbol{v}_s) &= 0. \end{aligned} \tag{3.20}$$

Under the assumption $\rho_n = \rho_n(s)$, we can at most write

$$\begin{aligned} \frac{\partial \rho_n}{\partial t} + \operatorname{div}(\rho_n \boldsymbol{v}_n) &= \Gamma, \\ \frac{\partial \rho_s}{\partial t} + \operatorname{div}(\rho_s \boldsymbol{v}_s) &= -\Gamma, \end{aligned} \tag{3.21}$$

where

$$\Gamma = \left(\overline{\rho}_n - \frac{\mathrm{d}\overline{\rho}_n}{\mathrm{d}s} s \right) \operatorname{div}(\rho_s \boldsymbol{v}_{ns}), \tag{3.22}$$

which is non-zero (even in the absence of heat sources or heat flux through boundary) since $\overline{\rho}_n$ is *not* linearly proportional to s. It could be tempting to design an SPH approximation by distinguishing super and normal particles, but the presence of "chemical reactions" between the two components (this also includes heating and cooling) does not make such idea favorable. This is accordance with a note by Landau, that superfluid helium is a material two motions rather than two components [59, 60].

3.3 Specific energy

Closing the system (3.15) requires the knowledge of $e = e(\rho, s, \boldsymbol{v}, \boldsymbol{v}_s)$, which satisfies (3.14). Unfortunately, a general energy formula appears to be missing in literature. However, using interpolation of experimental data, it is not difficult to derive a linear approximation near a reference temperature T_0. Doing such approximation is reasonable in most practical situations, because temperature of superfluid inside a cryostat rarely varies by more then a few milikelvins. To find that approximation, we begin by defining the kinetic part of specific energy as

$$e_{\text{kin}} := \frac{1}{2}\overline{\rho}_n v_n^2 + \frac{1}{2}\overline{\rho}_s v_s^2 = \frac{1}{2}v^2 + \frac{\overline{\rho}_s}{2\overline{\rho}_n}|\boldsymbol{v} - \boldsymbol{v}_s|^2. \tag{3.23}$$

Then

$$\mathrm{d}e_{\mathrm{kin}} = \boldsymbol{v}_n \cdot \mathrm{d}\boldsymbol{v} - \overline{\rho}_s \boldsymbol{v}_{ns} \cdot \mathrm{d}\boldsymbol{v}_s - \frac{v_{ns}^2}{2} \frac{\mathrm{d}\overline{\rho}_n}{\mathrm{d}s}\, \mathrm{d}s. \tag{3.24}$$

As a local approximation near referential specific entropy s_0, we assume constant $\gamma = \frac{\mathrm{d}\overline{\rho}_n}{\mathrm{d}s}$. That means

$$\begin{aligned} \overline{\rho}_n &= \overline{\rho}_{n0} + \gamma(s - s_0), \\ \overline{\rho}_s &= \overline{\rho}_{s0} - \gamma(s - s_0). \end{aligned} \tag{3.25}$$

The internal energy satisfies

$$\mathrm{d}e_{\mathrm{int}} = \mathrm{d}e - \mathrm{d}e_{\mathrm{kin}} = \left(T + \gamma \frac{v_{ns}^2}{2} \right) \mathrm{d}s + \frac{p}{\rho^2}\, \mathrm{d}\rho\,. \tag{3.26}$$

For lack of better knowledge, we assume simple linear relationship between p and ρ:

$$p = c_1^2(\rho - \rho_0) \tag{3.27}$$

where c_1 is the first speed of sound. In the absence of counterflow, we likewise assume a linear relationship between T and s:

$$T = T_0 \left(1 + \frac{s - s_0}{C_V} \right), \qquad (\boldsymbol{v}_{ns} = 0), \tag{3.28}$$

where C_V is the specific heat capacity at constant volume. (The off-diagonal dependence of (p, T) on (ρ, s) could be included, but the thermal expansion coefficient of superfluid helium is relatively small.) The expression (3.24) keeps the same form when we switch from variables $(\rho, s, \boldsymbol{v}, \boldsymbol{v}_s)$ to $(\rho, s, \boldsymbol{v}, \boldsymbol{v}_{ns})$. In these variables, we have a Maxwell relation:

$$0 = \frac{\partial}{\partial s} \frac{\partial e_{\mathrm{int}}}{\partial \boldsymbol{v}_{ns}} = \frac{\partial}{\partial \boldsymbol{v}_{ns}} \left(T + \gamma \frac{v_{ns}}{2} \right) = \frac{\partial T}{\partial \boldsymbol{v}_{ns}} + \gamma \boldsymbol{v}_{ns} \tag{3.29}$$

from which we infer how temperature is affected by the counterflow velocity when s and ρ are fixed. Thus, in the presence of counterflow, we find

$$T = T_0 \left(1 + \frac{s - s_0}{C_V} \right) - \frac{\gamma v_{ns}^2}{2}. \tag{3.30}$$

Note that the heat capacity is connected to the second speed of sound c_2 by (see [59]):

$$c_2^2 = \frac{\overline{\rho}_{s0} T_0 s_0^2}{\overline{\rho}_{n0} C_V}. \tag{3.31}$$

Integrating, we find a closed formula for potential energy in terms of ρ and s (fixing $e_{\mathrm{int}}(\rho_0, s_0) = 0$).

$$e_{\mathrm{int}} = c_1^2 \left(\ln\left(\frac{\rho}{\rho_0} \right) + \frac{\rho_0}{\rho} - 1 \right) + T_0 \left((s - s_0) + \frac{1}{2C_V} (s - s_0)^2 \right). \tag{3.32}$$

The constants $\overline{\rho}_{n0}, \overline{\rho}_{s0}, s_0, \gamma, \rho_0, c_1, c_2$ of this linear model for given referential temperature T_0 can be obtained from measured values (we refer to [53]).

3.4 Particle approximation

Similarly to the SHTC equations, we derive particle approximation from (3.11), which will allow us to verify conservation laws easily. Using the same notation for the discrete derivative, we write

$$\begin{aligned}\sum_a m_a \dot{u}_a = &\sum_a m_a \rho_a [e_{\rho,a} \operatorname{div}_a\{u_{\boldsymbol{v}} + u_{\boldsymbol{v}_s}\} - u_{\rho,a} \operatorname{div}_a\{e_{\boldsymbol{v}} + e_{\boldsymbol{v}_s}\}] \\ &- \sum_a m_a (\boldsymbol{v}_a - \boldsymbol{v}_{s,a}) \cdot [\nabla_a\{u_{\boldsymbol{v}}\} e_{\boldsymbol{v}_s,a} - \nabla_a\{e_{\boldsymbol{v}}\} u_{\boldsymbol{v}_s,a}] \\ &- \sum_a m_a s_a (\nabla_a u_s \cdot e_{\boldsymbol{v}_s,a} - \nabla_a\{e_s\} \cdot u_{\boldsymbol{v}_s,a}),\end{aligned} \tag{3.33}$$

which equivalently yields the following ODE system

$$\begin{aligned}\dot{\rho}_a &= -\rho_a \operatorname{div}_a\{\boldsymbol{v}\}, \\ \dot{s}_a &= -\frac{1}{\rho_a} \operatorname{div}^*_a(\rho\, \overline{\rho}_s s \boldsymbol{v}_{ns}), \\ \dot{\boldsymbol{v}}_a &= -\frac{1}{\rho_a} \operatorname{div}^*_a(\rho\, \overline{\rho}_s \overline{\rho}_n \boldsymbol{v}_{ns} \otimes \boldsymbol{v}_{ns}) - \frac{\nabla^*_a\{p\}}{\rho_a}, \\ \dot{\boldsymbol{v}}_{s,a} &= \overline{\rho}_{n,a} \nabla_a\{\boldsymbol{v}_n\}^T \boldsymbol{v}_{ns,a} - \frac{\nabla^*_a\{p\}}{\rho_a} + s_a \nabla_a T, \\ \dot{\boldsymbol{x}}_a &= \boldsymbol{v}_a\end{aligned} \tag{3.34}$$

Note that the system is consistent with the classical fluid limit, i.e. the SPH approximation for Eulerian fluid is recovered for $\overline{\rho}_n = 1$. (Except for an extra decoupled equation for $\boldsymbol{v}_s$. But when $\overline{\rho}_s = 0$, superfluid velocity does not contribute to the mass flow and its evolution becomes superfluous.) The conservation properties depend on a degree to which $\partial_a\{\cdot\}$ is exact.

Theorem 9. *Let $\rho_a(t)$, $s_a(t)$, $\boldsymbol{v}_a(t)$, $\boldsymbol{v}_{s,a}(t), \boldsymbol{x}_a(t)$ be C^1 solution of (3.34). Then*

1. *The total energy $\sum_a m_a e_a$ is conserved.*
2. *If $\partial_{a,i}\{\varphi\} = \partial_i \varphi(\boldsymbol{x}_a)$ for any constant function φ (zero-order consistency), then linear momentum is conserved and total entropy $\sum_a m_a s_a$ is conserved.*
3. *If $\partial_{a,i}\{\varphi\} = \partial_i \varphi(\boldsymbol{x}_a)$ for any linear function φ (first-order consistency), then angular momentum is conserved.*

Proof. Total energy preserved since the bracket vanishes when we set $u = e$ in (3.33). If the discrete derivative is first-order consistent, it allows us to set $u = \boldsymbol{v} \cdot \hat{\boldsymbol{x}}$ in (3.33), which gives

$$\begin{aligned}u_\rho &= u_s = 0, \\ u_{\boldsymbol{v}} &= \hat{\boldsymbol{x}}, \\ u_{\boldsymbol{v}_s} &= 0.\end{aligned} \tag{3.35}$$

The right-hand side of (3.33) vanishes since all terms are zero. This verifies conservation of x component of linear momentum. Conservation of other components

and entropy is performed similarly. If $\partial_{a,i}\{\varphi\} = \partial_i\varphi(\boldsymbol{x}_a)$ is first-order consistent, we can also set

$$\begin{aligned} u_\rho &= u_s = 0, \\ u_{\boldsymbol{v}} &= \hat{\boldsymbol{x}}y - \hat{\boldsymbol{y}}x, \\ u_{\boldsymbol{v}_s} &= 0. \end{aligned} \tag{3.36}$$

By design of the system, we easily find

$$\begin{aligned} \frac{\mathrm{d}}{\mathrm{d}t}\left(\sum_a m_a u_{\boldsymbol{v},a}\cdot\boldsymbol{v}_a\right) &= \sum_a m_a u_{\boldsymbol{v},a}\cdot\dot{\boldsymbol{v}}_a \\ &= \sum_a m_a\frac{p_a}{\rho_a}\operatorname{div}_a\{u_{\boldsymbol{v}}\} + \sum_a m_a\overline{\rho}_{s,a}\overline{\rho}_{n,a}\boldsymbol{v}_{ns,a}\cdot\nabla_a\{u_{\boldsymbol{v}}\}\boldsymbol{v}_{ns,a} \\ &= 0 \end{aligned} \tag{3.37}$$

since $\operatorname{div} u_{\boldsymbol{v}} = 0$, the matrix $\nabla u_{\boldsymbol{v}}$ is anti-symmetric, and the discrete derivative is exact for linear functions. This verifies conservation of z component of angular momentum. The proof is analogical for x and y components. □

There are two important irreversible forces in superfluid helium: viscosity of the normal component and vortex friction. The former can be implemented in the usual way using the Monaghan's viscous operator (1.81). The latter is more complicated and requires inclusion of at least one additional variable: the vortex line density (HVBK model). We will not follow this path here because it is still unclear how to incorporate vortex line density in Hamiltonian formulation of superfluid dynamics. This is unfortunate, since vortex friction might improve numerical stability. Until this problem is resolved, we recommend using a small parabolic diffusion to combat under-resolution of second sound. This results in irreversible part of equations in the following form:

$$\begin{aligned} \dot{\rho}_a &= 0, \\ \dot{s}_a &= 2\beta\sum_b m_b\frac{W'_{h,ab}}{r_{ab}}\frac{T_{ab}}{\rho_a\rho_b} + \frac{\zeta_a}{T_a\rho_a}, \\ \dot{\boldsymbol{v}}_a &= 2\mu(d+2)\sum_b m_b\frac{W'_{h,ab}}{\rho_a\rho_b r_{ab}}\,\frac{\boldsymbol{v}_{n,ab}\cdot\boldsymbol{x}_{ab}}{r_{ab}^2+\eta^2}\boldsymbol{x}_{ab}, \\ \dot{\boldsymbol{v}}_{s,a} &= 0, \\ \dot{\boldsymbol{x}}_a &= 0, \end{aligned} \tag{3.38}$$

where μ is dynamic viscosity coefficient, $\beta \geq 0$ is a small numerical parameter and the dissipative power ζ_a satisfies:

$$\zeta_a = -\beta\sum_b\frac{m_b}{\rho_b}\frac{W'_{h,ab}}{r_{ab}}T_{ab}^2 - \mu(d+2)\sum_b\frac{m_b}{\rho_b}\frac{(\boldsymbol{v}_{n,ab}\cdot\boldsymbol{x}_{ab})^2}{r_{ab}^2+\eta^2}\frac{W'_{h,ab}}{r_{ab}}. \tag{3.39}$$

Naturally, it is important to assure that the irreversible dynamics does not interfere with the conservative properties.

Theorem 10. *Let $\rho_a(t)$, $s_a(t)$, $\boldsymbol{v}_a(t)$, $\boldsymbol{v}_{s,a}(t), \boldsymbol{x}_a(t)$ be C^1 solution of* (3.38)*. Then the total energy is conserved, as well as linear momentum and angular momentum. Moreover, if the temperature and density are positive, the entropic inequality*

$$\frac{\mathrm{d}}{\mathrm{d}t}\left(\sum_a m_a s_a\right) \geq 0 \tag{3.40}$$

is satisfied.

Proof. Conservation of linear momentum follows from odd symmetry of the expression

$$\sum_a m_a \dot{\boldsymbol{v}}_a = 2\mu(d+2)\sum_{a,b} m_a m_b \frac{W'_{h,ab}}{\rho_a \rho_b r_{ab}} \frac{\boldsymbol{v}_{n,ab}\cdot \boldsymbol{x}_{ab}}{r_{ab}^2+\eta^2}\boldsymbol{x}_{ab} = 0. \tag{3.41}$$

In the proof of angular momentum conservation, we use the symmetrization trick, to infer:

$$\sum_a m_a \boldsymbol{x}_a \times \dot{\boldsymbol{v}}_a = \mu(d+2)\sum_{a,b} m_a m_b \frac{W'_{h,ab}}{\rho_a \rho_b r_{ab}} \frac{\boldsymbol{v}_{n,ab}\cdot \boldsymbol{x}_{ab}}{r_{ab}^2+\eta^2}\boldsymbol{x}_{ab} \times \boldsymbol{x}_{ab} = 0. \tag{3.42}$$

When it comes to the total energy, we find

$$\begin{aligned}
\sum_a m_a \dot{e}_a =& \sum_a m_a \left(\boldsymbol{v}_{n,a}\cdot \dot{\boldsymbol{v}}_a + m_a T_a \dot{s}_a\right) \\
=& \beta \sum_{a,b} m_a m_b \frac{W'_{h,ab}}{r_{ab}} \frac{T_{ab}^2}{\rho_a \rho_b} \\
&+ \mu(d+2)\sum_{a,b} m_b \frac{W'_{h,ab}}{\rho_a \rho_b r_{ab}} \frac{\left(\boldsymbol{v}_{n,ab}\cdot \boldsymbol{x}_{ab}\right)^2}{r_{ab}^2+\eta^2} \\
&+ \sum_a \frac{m_a \zeta_a}{T_a \rho_a} \\
=& 0
\end{aligned} \tag{3.43}$$

Finally, the total entropy obeys

$$\sum_a m_a \dot{s}_a = \sum_a \frac{m_a \zeta_a}{T_a \rho_a} \tag{3.44}$$

and it is clear that $\zeta_a \geq 0$ using non-increasing property of the smoothing kernel. □

The complete system is obtained by summing together the right-hand side of the reversible part (3.33) and the irreversible part (3.38). Obviously, the conservation properties and entropic inequality follow if assumptions of theorems 9 and 10 are satisfied. In examples below, only the zero-order consistent operators are employed to achieve smaller computation cost but sacrificing conservation of angular momentum. The closed expression for density (1.14) is used. To discretize time, we introduced the following extension of Verlet scheme, which has the time-reversal property when irreversible forces are absent.

0. (initial step only) find rate of $\boldsymbol{v}$ and $\boldsymbol{v}_s$

1. update $\boldsymbol{v}$ and $\boldsymbol{v}_s$ by $\frac{\delta t}{2}$ step
2. update $\boldsymbol{x}$ by $\frac{\delta t}{2}$ step
3. find ρ
4. find the rate of s
5. update s by δt step
6. update $\boldsymbol{x}$ by $\frac{\delta t}{2}$ step
7. find ρ
8. find the rate of $\boldsymbol{v}$ and $\boldsymbol{v}_s$
9. update $\boldsymbol{v}$ and $\boldsymbol{v}_s$ by $\frac{\delta t}{2}$ step

In each step, rates are evaluated using the most recent values of $s, \rho, \boldsymbol{v}, \boldsymbol{v}_s$ and $\boldsymbol{x}$.

3.5 Second sound waves

In the first example, we consider second sound which occurs in superfluid helium in the presence of heat sources. We will focus on mathematically simple case of two-dimensional second sound wave, for which approximate analytical solution can be found. The geometry of the problem is a square $\Omega = (0, L) \times (0, L)$, where $L = 1\text{cm}$. The boundaries are considered adiabatic

$$\boldsymbol{v}_n \cdot \boldsymbol{n} = 0, \quad \text{at } \partial\Omega \tag{3.45}$$

and no-slip condition on velocity is imposed

$$\boldsymbol{v} = 0, \quad \text{at } \partial\Omega. \tag{3.46}$$

If there is no co-flow in the initial state, it is reasonable to expect that the dynamics will be dominated by counter-flow. Hence, the ansatz $\boldsymbol{v} = 0$ and $\rho = \rho_0 = \text{const.}$ can be used to simplify two-fluid equations (3.15) as follows:

$$\begin{aligned} \frac{\partial \rho}{\partial t} &= 0 \\ \frac{\partial s}{\partial t} &= -\operatorname{div}(\overline{\rho}_s s \boldsymbol{v}_{ns}) \\ \frac{\partial \boldsymbol{v}}{\partial t} &= -\operatorname{div}(\overline{\rho}_s \overline{\rho}_n \boldsymbol{v}_{ns} \otimes \boldsymbol{v}_{ns}) \\ \frac{\partial \boldsymbol{v}_s}{\partial t} &= \overline{\rho}_n \nabla \boldsymbol{v}_n^T \boldsymbol{v}_{ns} + s \nabla T, \end{aligned} \tag{3.47}$$

if we further assume that counterflow velocity is small compared to L/t_{end}, we can further linearize for $\boldsymbol{v}_{ns} \approx 0$ and $s \approx s_0$. Hence, we find, to first order

approximation:

$$\begin{aligned}\frac{\partial \rho}{\partial t} &= 0\\ \frac{\partial s}{\partial t} &= -\overline{\rho}_{s0} s_0 \operatorname{div}(\boldsymbol{v}_{ns})\\ \frac{\partial \boldsymbol{v}}{\partial t} &= 0\\ \frac{\partial \boldsymbol{v}_s}{\partial t} &= s_0 \nabla T,\end{aligned} \tag{3.48}$$

The first and third equations witness that the ansatz is consistent. Combining the second and last equation with the relation for temperature (3.30) and with

$$\boldsymbol{v}_{ns} = \frac{1}{\overline{\rho}_n}(\boldsymbol{v} - \boldsymbol{v}_s) = -\frac{1}{\overline{\rho}_n}\boldsymbol{v}_s \approx -\frac{1}{\overline{\rho}_{n0}}\boldsymbol{v}_s, \tag{3.49}$$

we obtain an equation

$$\frac{\partial^2 s}{\partial t^2} = c_2^2 \Delta s \tag{3.50}$$

which describes waves spreading in all directions with the speed of second-sound (3.31). As a test case, we may consider a standing wave of specific entropy

$$\frac{s(\boldsymbol{x}, t) - s_0}{s_0} = A \cos\left(\frac{\pi x}{L}\right) \cos\left(\frac{\pi y}{L}\right) \cos\left(\frac{\sqrt{2}\pi c_2 t}{L}\right). \tag{3.51}$$

Note that this is not a precise solution of two-fluid equations, where coflow and counterflow are coupled non-linearly and cannot be separated. However, we can test whether the SPH model is consistent with the linear approximation when the dimensionless amplitude A approaches zero. Additionally, since the energy flux through boundary is absent, the example provides a convenient benchmark for energy conservation law. Figure 3.2 shows the results for various values of A, spatial resolution N (simulation contains $N \times N$ particles) and temporal resolution M. The boundary was implemented using the dummy particle approach. We see from the results that the achieved error is below 1% over time interval $(0, \frac{\sqrt{2}L}{u_2})$, which corresponds to one full period. The achieved relative energy error was 10^{-7}.

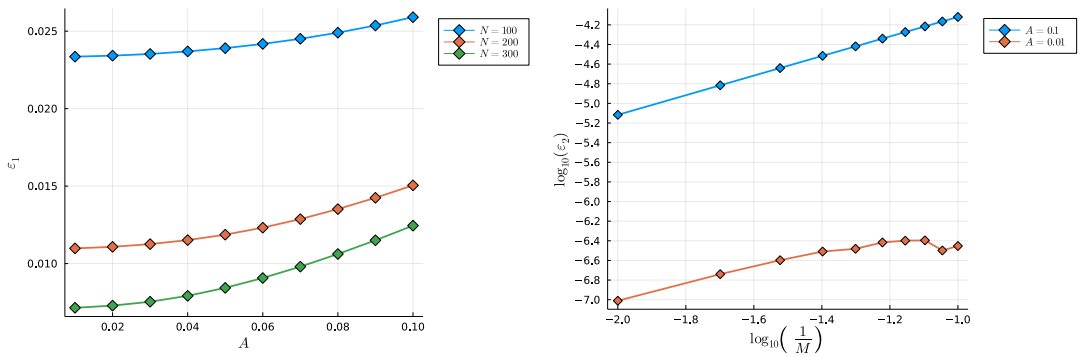

Figure 3.2: Left: relative error in entropy for $M = 50$ and different values of A, N. Right: energy error for $N = 200$ and different values of M and A.

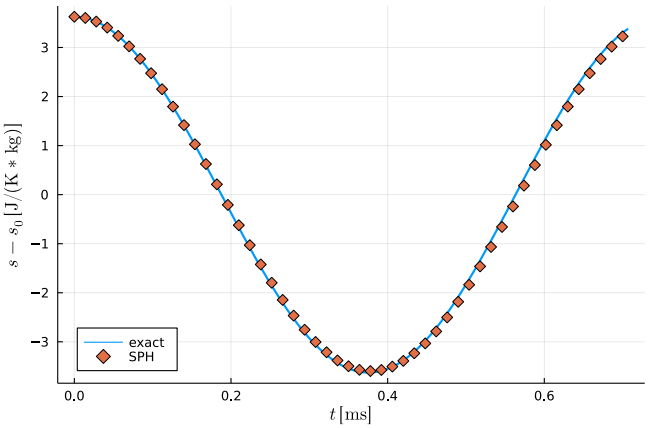

Figure 3.3: Evolution of entropy at $x = y = \frac{L}{4}$ in a simulation compared to the formula (3.51). Result for $A = 0.01$, $M = 50$ and $N = 300$.

3.6 Fountain effect

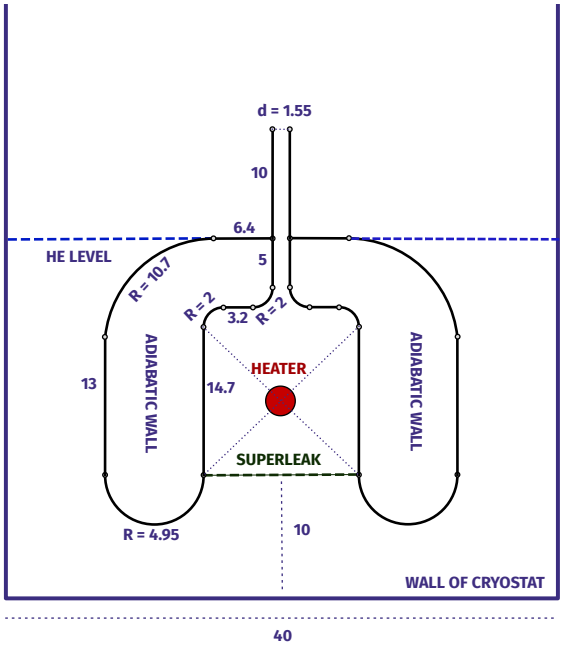

Figure 3.4: Scheme of the simulated apparatus. All lengths are expressed in millimeters. Shape is composed of line segments and circular sections with indicated radii.

A more sophisticated example is the superfluid fountain. Setup of the problem is depicted in Figure 3.4. A cell is submerged in superfluid helium and insulated by a *superleak* from the reservoir (cryostat). Superleak is a special layer, typically made of carbon silicates, which contains mesoscopic pores [61]. Such material stops the normal flow but is permeable to the inviscid superflow. We let side walls of the cell to be completely tight and adiabatic. A heat source of power $\dot{W}$ is contained in the cell. When the cell is heated, the mechano-caloric force accelerates superfluid velocity from the resorvoir upwards. If there was no superleak,

superflow would be balanced by opposite normalflow, resulting in zero momentum and only waves of second sound could be observed. The superleak, however, prevents the formation of this equilibrium, which results in over-pressure inside the cell. Heating the cell only by few millikelvins above the reservoir temperature T_0 generates sufficient pressure to power a jet through capillary. In an experiment, the problem would typically have cylindrical symmetry, but here, we will assume translational symmetry for simpler two-dimensional computation. We also assume a Dirichlet boundary condition for temperature $T = T_0$ on cryostat walls. Without this condition, the energy would not be extracted, resulting in steadily increasing temperature. Superleak can be implemented as a stiff external friction term, which does not affect $\boldsymbol{v}_s$. In total, the mathematical formulation is

$$\begin{aligned}
\dot{\rho} &= -\rho \operatorname{div} \boldsymbol{v} \\
\dot{s} &= -\frac{1}{\rho} \operatorname{div}(\rho\, \overline{\rho}_s s \boldsymbol{v}_{ns}) + \frac{\mu}{\rho T} |\mathbb{D}_n|^2 + \frac{1}{T\rho} \zeta_{\text{heat}} - \frac{1}{T} \boldsymbol{f}_{\text{superleak}} \cdot \boldsymbol{v}_n, \\
\dot{\boldsymbol{v}} &= -\frac{1}{\rho} \operatorname{div}(\rho\, \overline{\rho}_s \overline{\rho}_n \boldsymbol{v}_{ns} \otimes \boldsymbol{v}_{ns}) - \frac{\nabla p}{\rho} + \frac{1}{\rho} \operatorname{div}(2\mu \mathbb{D}_n) + \boldsymbol{g} + \boldsymbol{f}_{\text{superleak}}, \\
\dot{\boldsymbol{v}}_s &= \overline{\rho}_n \nabla \boldsymbol{v}_n^T \boldsymbol{v}_{ns} - \frac{\nabla p}{\rho} + s \nabla T + \boldsymbol{g}, \\
\boldsymbol{v} &= 0 \quad \text{at } \Gamma_{\text{adiabatic}} \cup \Gamma_{\text{cooler}}, \\
\boldsymbol{v}_n \cdot \boldsymbol{n} &= 0 \quad \text{at } \Gamma_{\text{adiabatic}}, \\
T &= T_0 \quad \text{at } \Gamma_{\text{cooler}},
\end{aligned} \tag{3.52}$$

where ζ is power density of heater, $\boldsymbol{f}_{\text{superleak}}$ is friction in superleak,

$$\mathbb{D}_n = \frac{1}{2}(\nabla \boldsymbol{v}_n + \nabla \boldsymbol{v}_n^T) \tag{3.53}$$

is the velocity deformation tensor and $\boldsymbol{g}$ is acceleration by gravity.

Jet speed of the fountain can be predicted analytically. To this end, we integrate balance of entropy over the cell volume Ω_{cell} (using the equivalent formulation (3.16) for entropy flux):

$$\begin{aligned}
\int_{\Omega_{\text{cell}}} \frac{\partial(\rho s)}{\partial t} \mathrm{d}\boldsymbol{x} = &- \int_{\Omega_{\text{cell}}} \operatorname{div}(\rho s \boldsymbol{v}_n) \mathrm{d}\boldsymbol{x} + \int_{\Omega_{\text{cell}}} \frac{2\mu}{T} |\mathbb{D}_n|^2 \mathrm{d}\boldsymbol{x} + \int_{\Omega_{\text{cell}}} \frac{1}{T} \zeta_{\text{heat}} \mathrm{d}\boldsymbol{x}. \\
&- \int_{\Omega_{\text{cell}}} \frac{1}{T} \boldsymbol{f}_{\text{superleak}} \cdot \boldsymbol{v}_n \mathrm{d}\boldsymbol{x}
\end{aligned} \tag{3.54}$$

In a stationary fountain, the left-hand side of (3.54) is zero. Let us neglect the entropy production terms on the right-hand side (on the basis that μ is very small) and invoke the Gauss theorem to obtain

$$\begin{aligned}
&\int_{\Gamma_{\text{adiabatic}}} \rho s \boldsymbol{v}_n \cdot \boldsymbol{n} \,\mathrm{d}S + \int_{\Gamma_{\text{superleak}}} \rho s \boldsymbol{v}_n \cdot \boldsymbol{n} \,\mathrm{d}S + \int_{\Gamma_{\text{capillary}}} \rho s \boldsymbol{v}_n \cdot \boldsymbol{n} \,\mathrm{d}S \\
&= \int_{\Omega_{\text{cell}}} \frac{1}{T} \zeta_{\text{heat}} \mathrm{d}\boldsymbol{x}
\end{aligned} \tag{3.55}$$

Since $\boldsymbol{v}_n = 0$, the integral on adiabatic wall is zero. Also, we neglect $\boldsymbol{v}_n$ in the superleak (since superleak, by definition, stops normalflow) and counterflow $\boldsymbol{v}_{ns}$

through capillary (where we expect a purely coflow jet). Moreover, due to the excellent heat conduction, s and T can be considered approximately constant within the cell. Thus, we find:

$$Q_{\text{capillary}} = \frac{\dot{W}_{\text{heater}}}{s_{\text{cell}} T_{\text{cell}}}, \tag{3.56}$$

where $\dot{W}_{\text{heater}}$ is power of heater and $Q_{\text{capillary}}$ is mass flux through capillary. (In the translationally symmetric example presented here, $Q_{\text{capillary}}$ is measured in kilograms per second per meter and $\dot{W}_{\text{heater}}$ in Watts per meter.) Although the formula (3.56) is very simple, it is found to be in good agreement with experiments [49]. Average jet velocity is related to the mass flow by

$$\boldsymbol{v}_{\text{jet}} = \frac{Q}{\rho_0 |\Gamma_{\text{capillary}}|} \tag{3.57}$$

In the discretization, we choose the following expression for superleak friction:

$$\boldsymbol{f}_{\text{superleak}} = -\frac{\overline{\rho}_{n,a} \boldsymbol{v}_{n,a}}{\tau_{\text{superleak}}} \left(W_H * \delta_{\{y=y_{\text{superleak}},\, |x| \leq r_{\text{superleak}}\}} \right) (\boldsymbol{x}_a), \tag{3.58}$$

where W_H is a kernel with smoothing length H and $\tau_{\text{superleak}}$ is the relaxation time. For the heat source, we use

$$\zeta_{\text{heat,a}} = \dot{W} \left(W_H * \delta_{\{x=x_{\text{heat}},\, y=y_{\text{heat}}\}} \right) (\boldsymbol{x}_a) \tag{3.59}$$

The result at temperature $T = 1.65\text{K}$ and various values of $\dot{W}$ are visualized in Figure 3.7 and the onset of the fountain with temperature field in Figures 3.6 and 3.8. Figure 3.5 shows the comparison of measured mass flux Q compared to the theoretical estimate (3.56) and demonstrates satisfactory agreement.

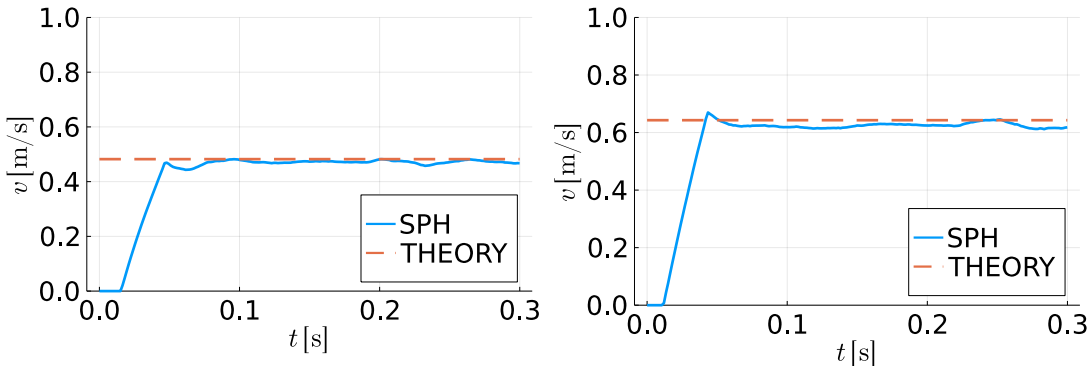

Figure 3.5: Evolution of the jet speed in comparison to theoretical prediction (3.56) for $\dot{W} = 60$ W/m (left) and for $\dot{W} = 80$ W/m (right). The discrepancy in the final state is about 2%.

3.7 Summary

In this section, a particle approximation of helium-four was derived from Hamiltonian formulation of superfluid dynamics. The system of equations was closed by an approximate energy formula, which is valid in the vicinity of referential temperature. We studied the conservation properties and tested the numerical approximation in a second sound benchmark. Finally, we successfully simulated a superfluid fountain.

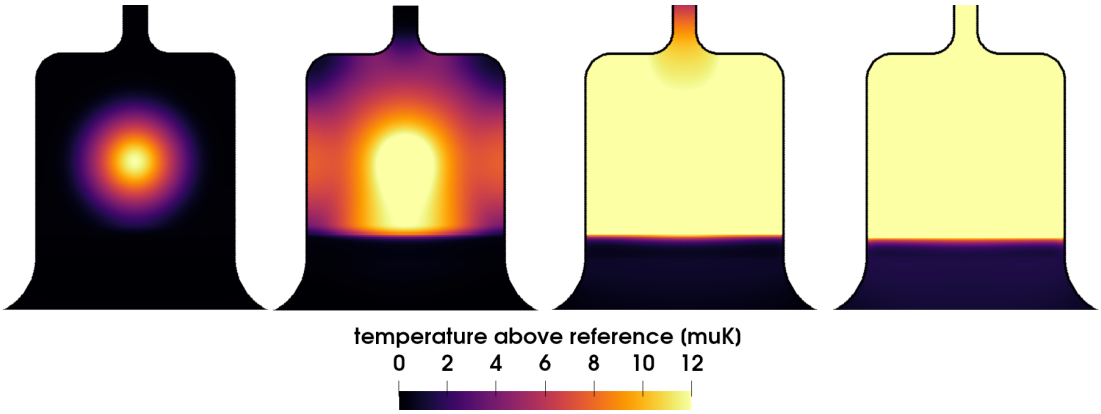

Figure 3.6: Plot of temperature inside the cell at $t = 0.25$, 0.5, 0.75 and 1ms (from left to right). We can see that the wave dynamics of second sound occurs on much shorter timescale than the total simulation length. In explicit SPH, such time scales are easy to resolve. This is because the time steps are already very short and computationally cheap.

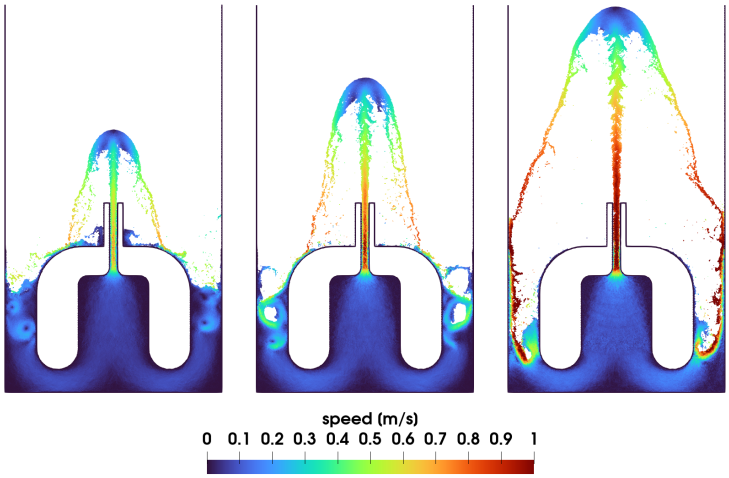

Figure 3.7: Plot of $\boldsymbol{v}$ magnitude at $t = 0.3$s for different values of heating power. From left to right: $\dot{W} = 60$, 80 and 100 W/m. Each simulation consists of approximately 200 000 particles. The jet speed and the height of the fountain matches analytical prediction.

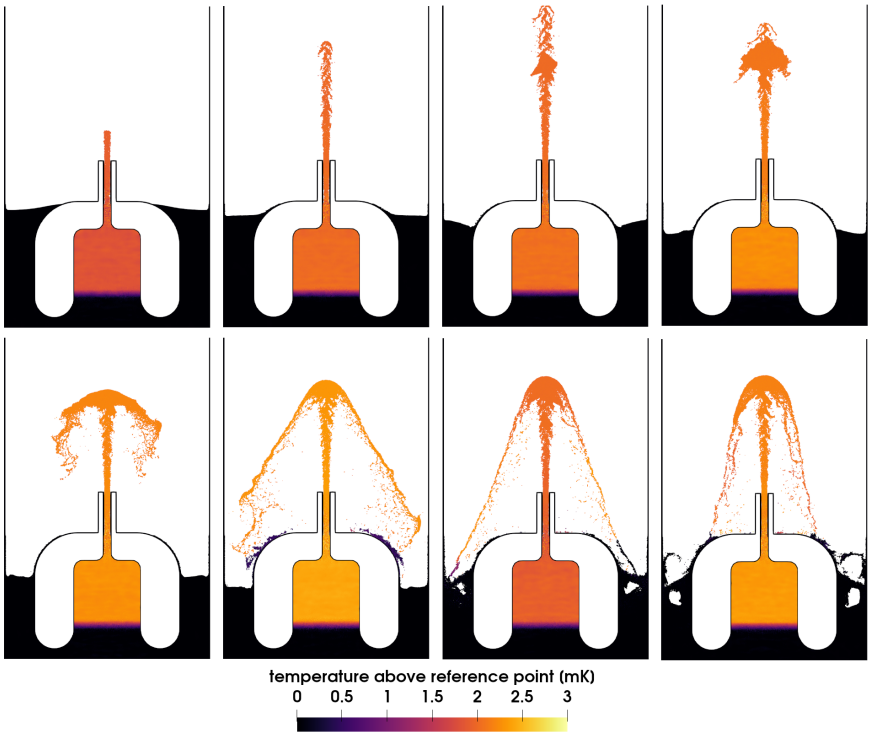

Figure 3.8: Plot of temperature distribution and fountain shape for $\dot{W} = 80\text{W/m}$ at equally spaced time frames from 37.5ms to 300ms. Due to excellent heat conduction in superfluid helium-4, temperature inside the cell is approximately constant after 1μs.

Conclusion

We presented novel geometric particle approximation of SHTC model and superfluid dynamics by discretizing their Poisson brackets. Our numerical models have many advantages, like easy implementation of free surface flows and very precise energy conservation. SPH approximation of SHTC allows for simulations of fluids and solids in a unified framework, where *fluidity* of a material is expressed by a single physical parameter, called relaxation time. Our ideas could be later extanded to other equations in Hamiltonian formulation, for example mixtures or equations of hyperbolic heat conduction.

Currently, a limitation of these results is the lack of theoretical foundation. Unfortunately, the error analysis for classical SPH portrayed in Chapter 1 cannot be used, because the discrete equations lack the strong form of consistency, where particle approximation can be interpreted as an exact distributional solution of a regularized system. Moreover, our time discretization schemes are heuristic and do not possess the advantages of symplectic integrators, since the equations themselves are not symplectic. Justification of the discrete approximation then relies on numerical experiments.

In the future, the particle approximation for SHTC model could be advantageously used in problems which combine free surface flows with phase change, such as simulations of additive manufacturing (3d printing) and mud flows. Applicability to non-Newtonian fluids and plastic solids remains to be investigated.

Regarding the particle approximation of the two-fluid model, our results open new opportunities for modeling low-temperature devices in time-dependent geometries. Particle simulation of a superfluid resonator appears as a promising direction of research. However, the model is so far incomplete because it does not feature evolution of vortex line density. Extension to HVBK model has not yet been investigated. Of interest is a possibility of mesoscopic particle model, which would simulate quantum turbulence on the level of vortex lines in an analogy to Vortex Filament Method.

Bibliography

[1] R.A. Gingold and J.J. Monaghan. Smoothed particle hydrodynamics: theory and application to non-spherical stars. *Mon. Not. R. Astron. Soc.*, 181(3):375–389, 1977.

[2] Joseph J Monaghan. SPH without a tensile instability. *Journal of computational physics*, 159(2):290–311, 2000.

[3] Larry D Libersky and Albert G Petschek. Smooth particle hydrodynamics with strength of materials. In *Advances in the Free-Lagrange Method Including Contributions on Adaptive Gridding and the Smooth Particle Hydrodynamics Method: Proceedings of the Next Free-Lagrange Conference Held at Jackson Lake Lodge, Moran, WY, USA 3–7 June 1990*, pages 248–257. Springer, 2005.

[4] Cornelius Lanczos. *The variational principles of mechanics*. Courier Corporation, 2012.

[5] Miroslav Grmela. GENERIC guide to the multiscale dynamics and thermodynamics. *Journal of Physics Communications*, 2(3):032001, 2018.

[6] Ondřej Kincl and Michal Pavelka. Globally time-reversible fluid simulations with smoothed particle hydrodynamics. *Computer Physics Communications*, 284:108593, 2023.

[7] Ondřej Kincl, Ilya Peshkov, Michal Pavelka, and Václav Klika. Unified description of fluids and solids in smoothed particle hydrodynamics. *Applied Mathematics and Computation*, 439:127579, 2023.

[8] Ondřej Kincl, David Schmoranzer, and Michal Pavelka. Simulation of superfluid fountain effect using smoothed particle hydrodynamics. *Physics of Fluids*, 35(4), 2023.

[9] Joseph J Monaghan and Robert A Gingold. *Journal of computational physics*, 52(2):374–389, 1983.

[10] Holger Wendland. Piecewise polynomial, positive definite and compactly supported radial functions of minimal degree. *Advances in computational Mathematics*, 4:389–396, 1995.

[11] JJ805872 Monaghan. Extrapolating B splines for interpolation. *Journal of Computational Physics*, 60(2):253–262, 1985.

[12] D. Violeau. *Fluid Mechanics and the SPH Method: Theory and Applications*. Oxford University Press, Oxford, UK, 2012.

[13] Joe J Monaghan. Smoothed particle hydrodynamics. *Annual review of astronomy and astrophysics*, 30(1):543–574, 1992.

[14] Matteo Antuono, Andrea Colagrossi, Salvatore Marrone, and Diego Molteni. Free-surface flows solved by means of sph schemes with numerical diffusive terms. *Computer Physics Communications*, 181(3):532–549, 2010.

[15] PB Tait. Report on some of the physical properties of fresh water and seawater, phys. *Chem. Voyag. HMS Chall. II Part IV*, 1888.

[16] Matteo Antuono, Andrea Colagrossi, Salvatore Marrone, and Claudio Lugni. Propagation of gravity waves through an SPH scheme with numerical diffusive terms. *Computer Physics Communications*, 182(4):866–877, 2011.

[17] Michal Pavelka, Václav Klika, and Miroslav Grmela. *Multiscale thermodynamics: introduction to GENERIC*. Walter de Gruyter GmbH & Co KG, 2018.

[18] Roberto Di Lisio, Emmanuel Grenier, and Mario Pulvirenti. The convergence of the SPH method. *Computers & Mathematics with applications*, 35(1-2):95–102, 1998.

[19] Andrea Colagrossi, Matteo Antuono, Antonio Souto-Iglesias, and David Le Touzé. Theoretical analysis and numerical verification of the consistency of viscous smoothed-particle-hydrodynamics formulations in simulating free-surface flows. *Physical Review E*, 84(2):026705, 2011.

[20] François Bolley. Separability and completeness for the Wasserstein distance. In *Séminaire de probabilités XLI*, pages 371–377. Springer, 2008.

[21] R Di Lisio, E Grenier, and M Pulvirenti. On the regularization of the pressure field in compressible euler equations. *Annali della Scuola Normale Superiore di Pisa-Classe di Scienze*, 24(2):227–238, 1997.

[22] Andrew Majda. *Compressible fluid flow and systems of conservation laws in several space variables*, volume 53. Springer Science & Business Media, 2012.

[23] Denis Donnelly and Edwin Rogers. Symplectic integrators: An introduction. *American Journal of Physics*, 73(10):938–945, 2005.

[24] Mark Kac. *Probability and related topics in physical sciences*, volume 1. American Mathematical Soc., 1959.

[25] Ronald D Ruth. A canonical integration technique. *IEEE Trans. Nucl. Sci.*, 30(CERN-LEP-TH-83-14):2669–2671, 1983.

[26] Haruo Yoshida. Construction of higher order symplectic integrators. *Physics letters A*, 150(5-7):262–268, 1990.

[27] Joseph P Morris, Patrick J Fox, and Yi Zhu. Modeling low Reynolds number incompressible flows using SPH. *Journal of computational physics*, 136(1):214–226, 1997.

[28] Joe J Monaghan. Smoothed particle hydrodynamics. *Annual review of astronomy and astrophysics*, 30(1):543–574, 1992.

[29] Ignacio Romero. Algorithms for coupled problems that preserve symmetries and the laws of thermodynamics: Part I: Monolithic integrators and their application to finite strain thermoelasticity. *Computer Methods in Applied Mechanics and Engineering*, 199(25-28):1841–1858, 2010.

[30] Seiichi Koshizuka and Yoshiaki Oka. Moving-particle semi-implicit method for fragmentation of incompressible fluid. *Nuclear science and engineering*, 123(3):421–434, 1996.

[31] Ilya Peshkov, Michal Pavelka, Evgeniy Romenski, and Miroslav Grmela. Continuum mechanics and thermodynamics in the Hamilton and the Godunov-type formulations. *Continuum Mechanics and Thermodynamics*, 30:1343–1378, 2018.

[32] Markus Hütter and Michal Pavelka. Particle-based approach to the Eulerian distortion field and its dynamics. *Continuum Mechanics and Thermodynamics*, pages 1–25, 2023.

[33] Ilya Peshkov, Michael Dumbser, Walter Boscheri, Evgeniy Romenski, Simone Chiocchetti, and Matteo Ioriatti. Simulation of non-Newtonian viscoplastic flows with a unified first order hyperbolic model and a structure-preserving semi-implicit scheme. *Computers & Fluids*, 224:104963, 2021.

[34] Petr Pelech, Karel Tůma, Michal Pavelka, Martin Šípka, and Martin Sỳkora. On compatibility of the natural configuration framework with general equation for non-equilibrium reversible–irreversible coupling (generic): Derivation of anisotropic rate-type models. *Journal of Non-Newtonian Fluid Mechanics*, 305:104808, 2022.

[35] Constantine M Dafermos and Constantine M Dafermos. *Hyperbolic conservation laws in continuum physics*, volume 3. Springer, 2005.

[36] I. E. Dzyaloshinskii and G. E. Volovick. Poisson brackets in condense matter physics. *Annals of Physics*, 125(1):67–97, 1980.

[37] Miroslav Grmela and Hans Christian Öttinger. Dynamics and thermodynamics of complex fluids. I. Development of a general formalism. *Phys. Rev. E*, 56:6620–6632, Dec 1997.

[38] Hans Christian Öttinger and Miroslav Grmela. Dynamics and thermodynamics of complex fluids. II. Illustrations of a general formalism. *Phys. Rev. E*, 56:6633–6655, Dec 1997.

[39] Michael Dumbser, Ilya Peshkov, Evgeniy Romenski, and Olindo Zanotti. High order ader schemes for a unified first order hyperbolic formulation of continuum mechanics: viscous heat-conducting fluids and elastic solids. *Journal of Computational Physics*, 314:824–862, 2016.

[40] MS El-Azab and Mohamed El-Gamel. A numerical algorithm for the solution of telegraph equations. *Applied Mathematics and Computation*, 190(1):757–764, 2007.

[41] Dean G Duffy. *Green's functions with applications*. cRc press, 2015.

[42] Michael L Falk and James S Langer. Dynamics of viscoplastic deformation in amorphous solids. *Physical Review E*, 57(6):7192, 1998.

[43] Walter Boscheri, Simone Chiocchetti, and Ilya Peshkov. A cell-centered implicit-explicit Lagrangian scheme for a unified model of nonlinear continuum mechanics on unstructured meshes. *Journal of Computational Physics*, 451:110852, 2022.

[44] UKNG Ghia, Kirti N Ghia, and CT Shin. High-re solutions for incompressible flow using the Navier-Stokes equations and a multigrid method. *Journal of computational physics*, 48(3):387–411, 1982.

[45] Steven W Van Sciver, KD Timmerhaus, and Alan F Clark. *Helium cryogenics*. Springer, 2012.

[46] David M Lee. The extraordinary phases of liquid 3 He. *Reviews of Modern Physics*, 69(3):645, 1997.

[47] G Klipping and H-D Denner. The thermo-mechanical effect of superfluid helium and its technical application. In *Advances in Cryogenic Engineering: Part A & B*, pages 81–93. Springer, 1990.

[48] JF Allen and H Jones. New phenomena connected with heat flow in helium II. *Nature*, 141(3562):243–244, 1938.

[49] María Lourdes Amigó, T Herrera, Lucas Neñer, L Peralta Gavensky, Federico Turco, and Javier Luzuriaga. A quantitative experiment on the fountain effect in superfluid helium. *European Journal of Physics*, 38(5):055103, 2017.

[50] Makoto Tsubota. Quantum turbulence: from superfluid helium to atomic Bose–Einstein condensates. *Contemporary physics*, 50(3):463–475, 2009.

[51] WF Vinen and JJ Niemela. Quantum turbulence. *Journal of low temperature physics*, 128:167–231, 2002.

[52] Ladislav Skrbek, David Schmoranzer, Šimon Midlik, and Katepalli R Sreenivasan. Phenomenology of quantum turbulence in superfluid helium. *Proceedings of the National Academy of Sciences*, 118(16):e2018406118, 2021.

[53] Russell J Donnelly and Carlo F Barenghi. The observed properties of liquid helium at the saturated vapor pressure. *Journal of physical and chemical reference data*, 27(6):1217–1274, 1998.

[54] L Landau. On the theory of superfluidity. *Physical Review*, 75(5):884, 1949.

[55] Martin Sỳkora, Michal Pavelka, Marco La Mantia, David Jou, and Miroslav Grmela. On the relations between large-scale models of superfluid helium-4. *Physics of Fluids*, 33(12):127124, 2021.

[56] Fritz London. *Superfluids: Macroscopic theory of superfluid helium*, volume 2. Dover Publications, 1954.

[57] Lev Davidovich Landau and Evgenii Mikhailovich Lifshitz. *Fluid Mechanics: Landau and Lifshitz: Course of Theoretical Physics, Volume 6*, volume 6. Elsevier, 2013.

[58] L Landau. On the vibrations of the electronic plasma. *Zhurnal eksperimentalnoi i teoreticheskoi fiziki*, 16(7):574–586, 1946.

[59] L. Landau. Theory of the superfluidity of helium II. *Phys. Rev.*, 60:356–358, 1941.

[60] L.D. Landau and E.M. Lifshitz. *Fluid Mechanics*. Number v. 6. Elsevier Science, 2013.

[61] David Linton Johnson and Pabitra N Sen. Multiple scattering of acoustic waves with application to the index of refraction of fourth sound. *Physical Review B*, 24(5):2486, 1981.

[62] Melvyn S Berger. *Nonlinearity and functional analysis: lectures on nonlinear problems in mathematical analysis*, volume 74. Academic press, 1977.

[63] H. Goldstein. *Classical Mechanics*. Pearson Education, 2002.

A. Functional derivatives and Poisson brackets

The following definition of functional derivative is used in the paper when deriving field equations from Poisson brackets:

Definition 3. *Let $D(\mathbb{R}^d)$ be the space of compactly supported smooth functions in d dimensions. Let*

$$F : D(\mathbb{R}^d) \to \mathbb{R} \tag{A.1}$$

be (possibly non-linear) functional. By $\delta F = \delta F(\varphi, \delta\epsilon)$, we denote the Gateaux derivative, i.e.:

$$\delta F(\varphi, \epsilon) = \lim_{h\to 0} \frac{F(\varphi + h\epsilon) - F(\varphi)}{h} \tag{A.2}$$

and call it functional differential of F at φ. In case there exists a distribution $g \in D'(\mathbb{R}^d)$ such that

$$\delta F(\varphi, \epsilon) = \langle g|\epsilon\rangle, \quad \forall \epsilon \in D(\mathbb{R}^d), \tag{A.3}$$

we write

$$g = \frac{\delta F}{\delta \varphi}(\varphi) \tag{A.4}$$

and call g the functional derivative of F at φ.

The definition trivially extends to cases when F is a function of more than one function or a vectorial function. We remind that even when the Gateaux derivative exists for any ϵ, there is no guarantee it will be linear. Even if it is linear, there is no guarantee that it will be continuous in $D'(\mathbb{R}^d)$ topology [62].

Example. Let F be a functional

$$F(\varphi) = \int f(\varphi(x), \nabla\varphi(x))\mathrm{d}\boldsymbol{x}, \tag{A.5}$$

where $f = f(x, \boldsymbol{y})$ is $C^2(\mathbb{R}\times\mathbb{R}^d)$ and $f(0,0) = 0$. In that case, we find

$$\frac{\delta F}{\delta\varphi} = \frac{\partial f}{\partial x} - \operatorname{div}\frac{\partial f}{\partial \boldsymbol{y}}. \tag{A.6}$$

In theoretical physics, *Poisson bracket* $\{\cdot,\cdot\}$ is a bilinear form, which accepts two functions of the phase space (and time) as arguments, yeilding a different function of phase space (and time). It satisfies the following identities:

- antisymmetry: $\{f, f\} = 0$,
- Leibniz rule: $\{f, gh\} = g\{f, h\} + h\{f, g\}$,
- Jacobi identity: $\{f, \{g, h\}\} + \{g, \{h, f\}\} + \{h, \{f, g\}\} = 0$,

for all functions f, g, h (satisfying some sort of regularity, depending on the context). Evolution of any function f in the phase space is determined by

$$\frac{\mathrm{d}f}{\mathrm{d}t} = \frac{\partial f}{\partial t} + \{f, E\}, \tag{A.7}$$

where E is total energy (Hamiltonian). In (A.7), the partial derivative $\frac{\partial f}{\partial t}$ is often not present unless f depends on time explicitly. In classical mechanics, Poisson bracket is

$$\{f, g\} = \frac{\partial f}{\partial q_i}\frac{\partial g}{\partial p_i} - \frac{\partial g}{\partial q_i}\frac{\partial f}{\partial p_i}, \tag{A.8}$$

where q_i are generalized coordinates and p_i are generalized momenta (summation over repeated index implied). Bracket (A.8) is called *canonical*. The notion naturally extends to continuum mechanics, where phase space has infinite dimensions and summation is replaced with an integral:

$$\{F, G\} = \int \left(\frac{\delta F}{\delta \chi_i}\frac{\delta G}{\delta M_i} - \frac{\delta G}{\delta \chi_i}\frac{\delta F}{\delta M_i} \right) \mathrm{d}\boldsymbol{x}, \tag{A.9}$$

where χ is the deformation map from reference to current frame and $\boldsymbol{M}$ is the momentum density in reference frame. For expression (A.9) to be well-defined, we not only require that functional derivatives of F and G exist, they also need to be L^2 functions [63].